

เครื่องสแกนเลเซอร์สามมิติเชิงภาพที่ใช้การแปลงเรขาคณิตสำหรับสร้างแบบจำลองสามมิติขึ้น
ใหม่



นางสาวพิมพ์ภัท หนูสุทธิยาภรณ์

ศูนย์วิทยทรัพยากร

วิทยานิพนธ์นี้เป็นส่วนหนึ่งของการศึกษาตามหลักสูตรปริญญาวิศวกรรมศาสตรมหาบัณฑิต

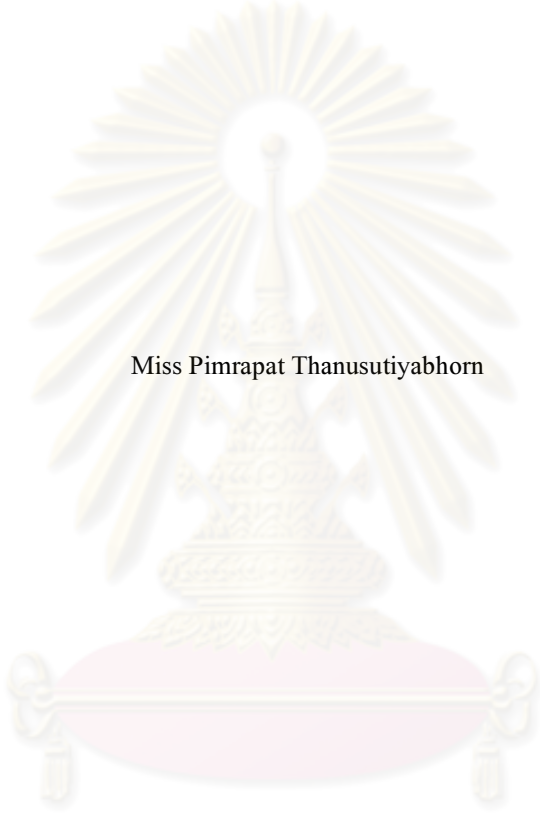
สาขาวิชาวิศวกรรมคอมพิวเตอร์ ภาควิชาวิศวกรรมคอมพิวเตอร์

คณะวิศวกรรมศาสตร์ จุฬาลงกรณ์มหาวิทยาลัย

ปีการศึกษา 2553

ลิขสิทธิ์ของจุฬาลงกรณ์มหาวิทยาลัย

IMAGE-BASED 3D LASER SCANNER USING GEOMETRIC TRANSFORMATION FOR
RECONSTRUCTING 3D MODELS



Miss Pimrapat Thanusutiyabhorn

ศูนย์วิทยทรัพยากร
จุฬาลงกรณ์มหาวิทยาลัย

A Thesis Submitted in Partial Fulfillment of the Requirements
for the Degree of Master of Engineering Program in Computer Engineering

Department of Computer Engineering

Faculty of Engineering

Chulalongkorn University

Academic Year 2010

Copyright of Chulalongkorn University

พิมพ์รภัศ ธนสุทธยาภรณ์ : เครื่องสแกนเลเซอร์สามมิติเชิงภาพที่ใช้การแปลง
เรขาคณิตสำหรับสร้างแบบจำลองสามมิติขึ้นใหม่. (IMAGE-BASED 3D LASER
SCANNER USING GEOMETRIC TRANSFORMATION FOR
RECONSTRUCTING 3D MODELS) อ. ที่ปรึกษาวิทยานิพนธ์หลัก: ผู้ช่วย
ศาสตราจารย์ ดร. พิษณุ คนองชัยศ.อ. ที่ปรึกษาวิทยานิพนธ์ร่วม: Waleed S.
Mohammed, Ph.D., 56หน้า.

เครื่องสแกนเนื้อหาดิจิตอลสามมิติเป็นเครื่องมือที่มีความสำคัญและมีประโยชน์
สำหรับการแสดงภาพหรือเนื้อหาสามมิติ อย่างไรก็ตาม เครื่องมือเหล่านี้มีราคาแพงเนื่องจาก
ตำแหน่งของกล้องและแหล่งกำเนิดแสงต้องถูกกำหนดอย่างแม่นยำตามหลักตรีโกณมิติ
นอกจากนี้เครื่องมือส่วนใหญ่ยังไม่เหมาะสำหรับการสแกนพื้นผิวที่มีความมันวาว งานวิจัยชิ้น
นี้เพื่อศึกษาระบบการสร้างรูปสามมิติจากเครื่องสแกนที่ราคาไม่แพงเพราะการสร้างและการ
ทำงานไม่ซับซ้อน การคำนวณข้อมูลสามมิติอาศัยข้อมูลจากรูปภาพที่ถ่ายมาเท่านั้น โดย
สามารถหาได้ด้วยการสร้างกล่องอ้างอิง หลักการทำงานและการคำนวณข้อมูลสามมิติเกิดจาก
การซ่อมแซมเนื้อหาในกรอบสี่เหลี่ยมที่เกิดการบิดเบือนแบบเชิงเส้น นอกจากนี้งานวิจัยนี้ยังได้
ศึกษาแนวทางการแก้ปัญหาการสแกนพื้นผิวที่มีความมันวาวโดยอาศัยความรู้เรื่องโพลาไรไร
เซชันของแสงและการประมวลผลภาพ ผู้วิจัยได้ทำการทดลองเพื่อวิเคราะห์ความสามารถใน
การทำงานของระบบสร้างรูปสามมิติที่เสนอรวมถึงข้อจำกัดต่างๆ จากผลการทดลองพบว่าวิธีที่
นำเสนออาจเป็นทางเลือกใหม่ให้กับการสร้างเครื่องสแกนสามมิติที่มีราคาไม่แพงและไม่
ซับซ้อน

ภาควิชา..วิศวกรรมคอมพิวเตอร์..... ลายมือชื่อนิติศ... Pimrapat T.....

สาขาวิชา..วิศวกรรมคอมพิวเตอร์... ลายมือชื่อ อ.ที่ปรึกษาวิทยานิพนธ์หลัก... P. K. J.....

ปีการศึกษา...2553..... ลายมือชื่อ อ.ที่ปรึกษาวิทยานิพนธ์ร่วม Waleed S.....

5270786721 : MAJOR COMPUTER ENGINEERING

KEYWORDS : 3D LASER SCANNER / 3D MODELS / IMAGE PROCESSING /
GEOMETRIC TRANSFORMATION

PIMRAPAT THANUSUTTYABHORN : IMAGE-BASED 3D LASER SCANNER
USING GEOMETRIC TRANSFORMATION FOR RECONSTRUCTING 3D
MODELS . ADVISOR : ASSISTANT PROFESSOR PIZZANU
KANONGCHAIYOS, Ph.D., CO-ADVISOR : WALEED S. MOHAMMED, Ph.D.,
56 pp.

3D scanner is an important tool for any fields that need to represent scenes or objects in 3D models. However, most of the commercial 3D scanners are expensive because the production of the machine has to be precisely built according to the triangulation concept. Moreover, most of them are not capable for scanning non-Lambertian surfaces. This thesis presents a 3D modeling system that is low cost and easy to setup. The complexity and the cost of the system are recuded by employing the image processing concept. This is done through the construction of a special design reference box that, monitored from the camera, will give information that is necessary for 3D reconstruction. The distorted area of interest is recovered using the geometric transformation under the assumption that the distortion is linear. The experiments were conducted to analyze the performance and the limitation of the method. Light polarization concept is also studied in this thesis. A linear polarizer was used to test the feasibility to distinguish the light that scattered from non-Lambertian surfaces. The results of the study show that the proposed 3D modeling system can be an alternative way for building a 3D scanner that is low cost and not complex.

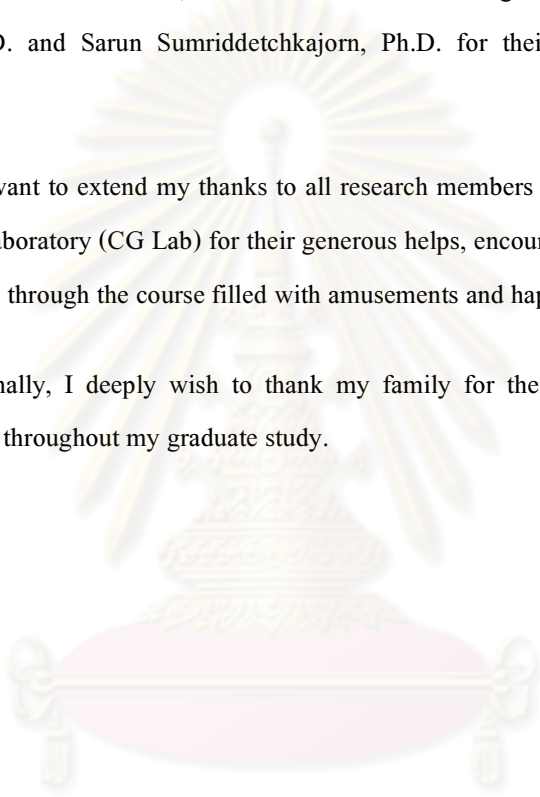
Department : Computer Engineering	Student's Signature <u>Pimrapat T.</u>
Field of Study : Computer Engineering	Advisor's Signature <u>Piz</u> <u>Kh</u>
Academic Year : 2010	Co-advisor's Signature <u>Waleed S.</u>

Acknowledgements

It is a great pleasure to acknowledge my thesis advisor, Assistant Professor Pizzanu Kanongchaiyos, Ph.D. and Waleed S. Mohammed, Ph.D. for their intellectual advices and invariable assistances throughout this research. I also would like to express my grateful thanks to my thesis committee, Professor Prabhas Chongstitvatana, Ph.D., Supatana Auethavekiat, Ph.D. and Sarun Sumriddetchkajorn, Ph.D. for their beneficial guidance and suggestions.

I want to extend my thanks to all research members especially my associates in computer graphic laboratory (CG Lab) for their generous helps, encouragements and relationships which make my life through the course filled with amusements and happiness.

Finally, I deeply wish to thank my family for their love, understanding and invaluable supports throughout my graduate study.



ศูนย์วิทยทรัพยากร
จุฬาลงกรณ์มหาวิทยาลัย

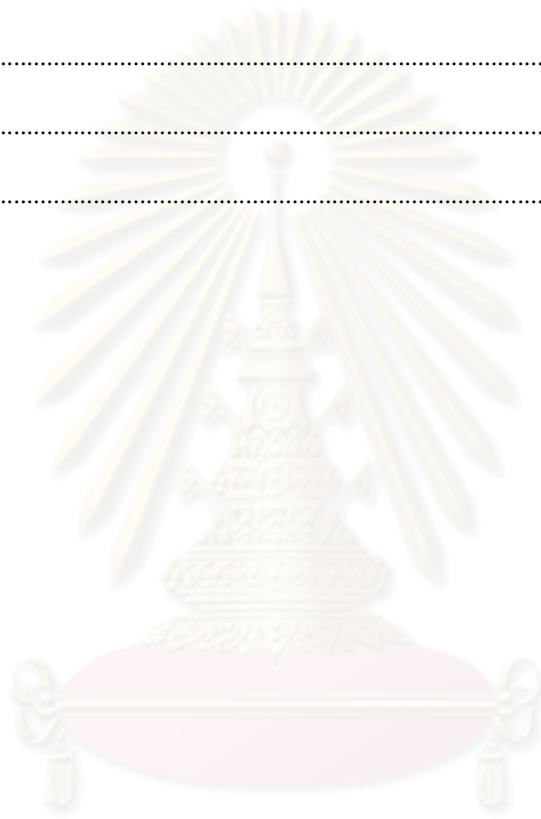
Contents

	PAGE
Abstract (THAI)	IV
Abstract (ENGLISH)	V
Acknowledgements	VI
Contents	VII
List of tables	XI
List of figures	XII
Chapter I Introduction	1
1.1. Background and statement of problem	1
1.2. Objective	2
1.3. Scope of study	2
1.4. Research procedure	3
1.5. Expected outcome	3
1.6. Thesis structure	4
1.7. Publication	4
Chapter II Theoretical background and related works	5
2.1. Theoretical background	5
2.1.1. Digital Image Processing	5
2.1.2. Light polarization	8
2.1.3. Iterative Closest Point (ICP) algorithm	9
2.1.4. Hausdorff distance	10
2.2. Related works	10
2.2.1. Laser peak detection methods	11

2.2.2.	3D scanner technology.....	11
2.2.3.	Less complex 3D scanner	12
2.2.4.	Scanning non-Lambertian surface	13
2.2.5.	Summary	15
Chapter III	3D scanning system	16
3.1.	Overview of 3D scanning system	16
3.2.	3D laser scanner design.....	17
3.3.	Algorithm and data.....	18
3.3.1.	Data acquisition	18
3.3.2.	Image Processing	19
3.3.4.	Registration.....	22
Chapter IV	Experimental results and discussion	24
4.1.	Overview of the experiments	24
4.2.	Measurement of the accuracy of recovering the original points	24
4.2.1.	Notation	24
4.2.2.	Task.....	25
4.2.3.	Equipments	25
4.2.4.	Hypothesis	25
4.2.5.	Variables	25
4.2.6.	Procedures.....	26
4.2.7.	Experimental results	27
4.3.	Measurement of the accuracy of 3D reconstruction on primitive models	28
4.3.1.	Notation	29
4.3.2.	Task.....	29

4.3.3.	Equipments	30
4.3.4.	Hypothesis	30
4.3.5.	Variables	30
4.3.6.	Procedures.....	30
4.3.7.	Experimental results	31
4.4.	Measurement of time spent on reconstructing a complete 3D model.....	32
4.4.1.	Notation	32
4.4.2.	Task.....	32
4.4.3.	Equipments	32
4.4.4.	Hypothesis	33
4.4.5.	Variables	33
4.4.6.	Procedures.....	33
4.4.7.	Experimental results	33
4.5.	Comparing the effect of applying linear polarizer on the light characteristic when reflected on non-Lambertian surfaces.....	35
4.5.1.	Notation	35
4.5.2.	Task.....	36
4.5.3.	Equipments	36
4.5.4.	Hypothesis	36
4.5.5.	Variables	36
4.5.6.	Procedures.....	37
4.5.7.	Experimental results	37
4.6.	Discussion	38
Chapter V	Conclusion and future work.....	41
5.1.	Conclusion.....	41

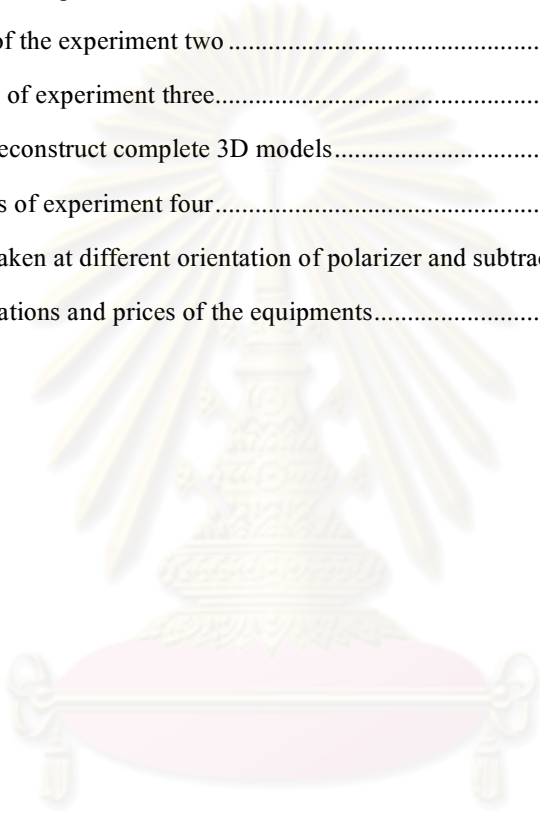
	X
5.2. Future works.....	42
References.....	43
APPENDICES	46
APPENDIX A.....	47
APPENDIX B.....	50
APPENDIX C	52
Biography.....	56



ศูนย์วิทยทรัพยากร
จุฬาลงกรณ์มหาวิทยาลัย

List of tables

	PAGE
Table 4-1: Variables of the experiment one.....	26
Table 4-2 Variables of experiment two.....	30
Table 4-3: Results of the experiment two.....	31
Table 4-4 Variables of experiment three.....	33
Table 4-5 Time to reconstruct complete 3D models.....	34
Table 4-6: Variables of experiment four.....	36
Table 4-7: Images taken at different orientation of polarizer and subtracted images.....	38
Table B-1: Specifications and prices of the equipments.....	51


 ศูนย์วิทยทรัพยากร
 จุฬาลงกรณ์มหาวิทยาลัย

List of figures

	PAGE
Figure 2-1: Representing digital image.....	5
Figure 2-2: The full color image and its three extracted components (red, green and blue).....	6
Figure 2-3: Corresponding tie-points in two images	8
Figure 2-4: Two orthogonal components forming the polarization state of the light wave.....	9
Figure 2-5: Laser stripe on (a) Lambertian Surface (b) Translucid	11
Figure 2-6: Experimental result [9] (a) Image of true laser stripe with inter-reflection created by a cylindrical hole in a metal surface (b) Discrimination of true stripe from inter-reflection	14
Figure 2-7: Experimental result [12] (a) Scene (b) Phase-shifting (c) Parallel polarization (d) PDI	14
Figure 3-1: Process of recovering the distorted image	17
Figure 3-2: Conceptual 3D Laser Scanner.....	18
Figure 3-3: Captured images with the presenting of tie-points.....	18
Figure 3-4: Converting RGB color image to intensity image.....	19
Figure 3-5: Algorithm of reference lines defining	20
Figure 3-6: Parameters defining.....	21
Figure 3-7: Algorithm of image processing in each frame for 3D modeling	21
Figure 3-8: 3D point cloud presented by Meshlab [22].....	22
Figure 3-9: Point cloud registration	23
Figure 4-1: Images (-45 degree tilted in z-axis) taken at four different distances	27
Figure 4-2: The graph presenting percent error of absolute distance and the distance.....	28
Figure 4-3: The configuration of the scene captured by a camera (d=60cm) (a) best case (b) average case (c) worst case	28
Figure 4-4: The colorized 3D reconstructed models (a) the best case (b) the average case (c) the worst case	32
Figure 4-5: The chart represents the time spent on reconstructing complete 3D models.....	35
Figure A-1: Images set of Case1	47
Figure A-2: Images set of Case2.....	47

Figure A-3: Images set of Case3.....	48
Figure A-4: Images set of Case4.....	48
Figure A-5: Images set of Case5.....	49
Figure A-6: Images set of Case6.....	49
Figure B-1: 3D Laser Scanner	50
Figure B-2: Images of the setup components (a) laser source (b) cylindrical lens (c) translation stage (d) camera (e) reference box.....	50
Figure C-1: Real object and reconstructed 3D models of orthogonal planes	52
Figure C-2: Real object and reconstructed 3D models of cylinder.....	52
Figure C-3: Real object and reconstructed 3D models of rectangular box.....	53
Figure C-4: Real object and reconstructed 3D models of cone	53
Figure C-5: Real object and reconstructed 3D models of sphere	53
Figure C-6: Real object and reconstructed 3D models of paper cup	54
Figure C-7: Real object and reconstructed 3D models of toy.....	54
Figure C-8: Real object and reconstructed 3D models of banana.....	55
Figure C-9: Real object and reconstructed 3D models of toy.....	55

Chapter I

Introduction

1.1. Background and statement of problem

Due to the growing demand of representing scenes or objects in 3D models that is applicable in many fields, noncontact optical surface digitizers, also known as 3D range sensors, have been developed enormously [1]. 3D range sensor or 3D scanner is a device that is used to analyze a real world object or scene and collect its shape in 3D model. A digital 3D computer model of the objects can be reconstructed and stored in a digital library which later can be applicable in many fields such as in academic, arts preserving or entertainment industries.

Cultural Heritage is one of the fields that employ the 3D range sensors technologies in research and study [2]. Khon is a Thai classical masked dance which is performed by non-speaking casts such that the characters have to be portrayed by the performance and unique costumes. These costumes including masks, clothes and ornaments are mostly hand-made and very detailed. It is always important to preserve this form of art in every aspect for the new generations. Hence, 3D models of these costumes and ornament can be one efficient way to preserve this form of arts. 3D scanning technologies work by collecting the profile of an object's surface digitally. The digital 3D data of the surface is then reconstructed into a 3D CAD model.

Many research works about 3D range finding system focus on the ranging method techniques and the algorithms used for computing the data, noise reduction or alignment. Most of this focuses on the development of ranging methods restricting to two main principles: Time-of-Flight (TOF) or Triangulation. The accuracy of such systems highly depends on the camera and light source calibration processes which are essentially needed [3]. The dependence on the relative location of the camera and light source and related parameters increases the cost of the system due to the need of complicated mechanical parts [3].

Another problem occurring from using such methods is when applying the system with high reflective, translucent or transparent objects. The line deformation becomes harder to be observed because of the light might travel through or reflect in a way that cannot be captured by the

camera. This leads to wrong calculation of the depth or in the worst case failing to interpret data. The method that is commonly used to solve the problem is spraying the part with matte paint. This cannot be applied in Khon scanning due to the permanent object damage. Many researches have been carried on solving the problem of scanning these types of objects. Applying optical knowledge or computer vision, high reflective or non-opaque objects can be successfully reconstructed.

The focus of this research is to develop a new way of a low-cost 3D modeling system and to demonstrate its potential values in scanning various objects including some that surfaces are non-Lambertian. The key inspiration of this work is to formulate a new way of 3D reconstruction that does not depend on the correspondence between the camera, object and light source. This is done through the construction of a special reference box to eliminate the pre-calibration process. Hence, the method becomes purely based on image processing of each frame from which the data for 3D computation are directly reconstructed.

1.2. Objective

This thesis aims to build an in-house 3D laser scanning system that can be used to reconstruct real world objects. The system can reconstruct the 3D point cloud of the objects correctly. The 3D point cloud of the object can be exported and used with mesh processing software.

1.3. Scope of study

This thesis focuses on building a 3D scanning system that can be used to scan real world objects. The proposed system consists of the laser scanner prototype and software for 3D reconstruction. The proposed method of 3D reconstruction is purely based on image processing which save the cost and reduce the complexity of the system. The software is implemented on MATLAB R2009a. The registration process is not included in this thesis.

1.4. Research procedure

1.4.1. Literature review

1.4.2. Related theories

1.4.2.1. Digital Image Processing Concepts

1.4.2.2. Optics theories

1.4.2.3. Iterative Closest Point (ICP) algorithm

1.4.2.4. Hausdorff distance

1.4.3. Previous research studies, articles, books and online information technology

1.4.4. Designing the system

1.4.5. Building the 3D laser scanner prototype

1.4.6. Designing an algorithm

1.4.7. Program development

1.4.8. Experiments

1.4.9. Analysis

1.4.10. Deliverables and conclusion

1.5. Expected outcome

The proposed 3D scanner system is easy for the user to set up and low cost. The scanner should be able to scan real world objects and some non-Lambertian surface objects without spraying the matt-paint. The proposed 3D modeling method can give less than 10 percent RMS error at the scale of centimeter.

1.6. Thesis structure

This thesis consists of five chapters and three appendices

Chapter 1 introduces the overview of the thesis which provides some background, motivation, the objective, scope of study, expected outcome and thesis structure.

Chapter 2 introduces some theoretical background and related works. This chapter provides some mathematics of image processing, optical knowledge and error analysis. The related works is divided into four different research questions which are the peak detection method, 3D scanner technology, less complex 3D scanner and 3D scanning on non-Lambertian surfaces using light polarization concept.

Chapter 3 explains the proposed 3D scanning system purely based on image processing concept. This chapter is sub-divided into three parts: overview of 3D scanning system, 3D laser scanner design and algorithm and data.

Chapter 4 demonstrates the experimental results and discussion. There are four experiments have been done in this thesis. The first experiment is to see the effect of the set up configuration on the accuracy of the recovered data. The second experiment is to measure the accuracy of the proposed method on primitive objects. The third experiment is to measure the time to reconstruct complete 3D models. The fourth experiment is to see the light polarization effect when the laser stripe was shone on non-Lambertian surfaces.

Chapter 5 summarizes the thesis and suggests some future works that can extended from this thesis.

1.7. Publication

Some parts of this research have been accepted to be published in the Proceedings of ECTI-CON-2011 and will be available via IEEE Xplore. The conference will be held on May 17-19, 2011 at Khon Kaen, Thailand. The paper title is “Image-based 3D Laser Scanner”. The authors are Pimrapat Thanusutiyabhorn, Pizzanu Kanongchaiyos and Waleed S. Mohammed.

Chapter II

Theoretical background and related works

This chapter consists of two parts. The first part mainly talks about the fundamental theories and concepts that are related to the proposed 3D scanning system. The second part discusses some previous research works aiming to solve the problem in different areas.

2.1. Theoretical background

2.1.1. Digital Image Processing

This section covers some basics of digital image processing, light polarization, iterative closest point algorithm and image comparison using Hausdorff Distance

2.1.1.1. Representing digital image

The digital images are generally represented by a matrix of real numbers [4]. An image $f(x, y)$ has M rows and N columns and each element in the matrix is called pixel. $f(x, y)$ is a function that assigns a gray-level value (usually 8-bit). The values of the coordinates (x, y) are discrete quantities and presented by integer values. The coordinates at the origin are $(x, y) = (0, 0)$. Figure 2-1 shows the coordinate convention used in this research.

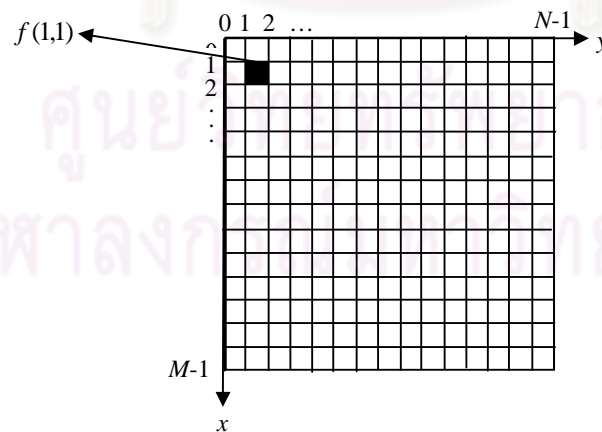


Figure II-1: Representing digital image

2.1.1.2. RGB to Intensity image

In general, many images are presented using different color models such as RGB, CMYK or HIS [4]. Images represented in the RGB color model consist of three components images, one for each primary color: red, green and blue. The pixel depth of color images is 24 bits, 8 bits for each color component. Each component image is represented by a monochrome image whose intensity is proportional to the response of that filter [4]. Figure 2-2 shows a full color image and its three components.

A grayscale image (or intensity image) is an image in which the value of each pixel carries only intensity information (8 bits). The conversion of a color image to grayscale image can be performed by forming a weighted sum of red, green and blue components in each pixel as shown in equation 2-1 [5]. Where $I(x,y)$ is the intensity value of the pixel. f_{red} , f_{green} and f_{blue} are the gray scale value of the pixel in red, green and blue components respectively.

$$I(x,y) = 0.2989 \times f_{red}(x,y) + 0.5870 \times f_{green}(x,y) + 0.1140 \times f_{blue}(x,y) \quad (II-1)$$

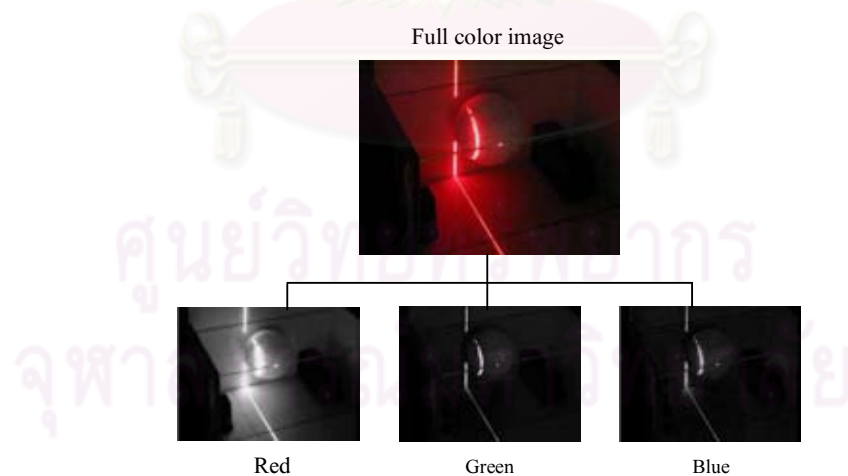


Figure II-2: The full color image and its three extracted components (red, green and blue)

2.1.1.3. Geometric transformation

Geometric transformations modify the spatial relationships between pixels in an image. It consists of two basic operations: a spatial transformation and gray-level interpolation. Spatial transformation defines the rearrangement of pixels on the image plane. Gray-level interpolation deals with the assignment of gray levels to pixels in the spatially transformed images. In this paper, we only focus on the spatial transformation [4]. The 3D reconstruction method proposed in this thesis employs the spatial transformation to recover the distorted data captured from a camera.

Suppose that an image $f(x, y)$ undergoes geometric distortion to produce an image $g(x', y')$. The transformation can be expressed as

$$\mathbf{x}' = \mathbf{r}(\mathbf{x}, \mathbf{y}) \quad (\text{II-2})$$

and

$$\mathbf{y}' = \mathbf{s}(\mathbf{x}, \mathbf{y}) \quad (\text{II-3})$$

Where $r(x, y)$ and $s(x, y)$ are the spatial transformations that produce the geometrically distorted image $g(x, y)$ [4]. Theoretically, it is possible to recover $f(x, y)$ from the distorted image $g(x, y)$ by applying the transformation in reverse. However, formulating set of analytical functions $r(x, y)$ and $s(x, y)$ that describe the geometric distortion process over the entire image are generally impossible [4]. In practice, the difficulty can be resolved by formulating the spatial relocation of pixels by use of tie-points, which are a subset of pixels whose location in the input (distorted) and output (corrected) images is known precisely. Figure 2-3 shows quadrilateral regions in a distorted and corresponding corrected image. The vertices of the quadrilaterals are corresponding tie-points. Suppose that the geometric distortion process within the quadrilateral regions is modeled by a pair of bilinear equations as shown in equations 2-4 and 2-5 [4].

$$\mathbf{r}(\mathbf{x}, \mathbf{y}) = \mathbf{x}' = \mathbf{c}_1\mathbf{x} + \mathbf{c}_2\mathbf{y} + \mathbf{c}_3\mathbf{x}\mathbf{y} + \mathbf{c}_4 \quad (\text{II-4})$$

and

$$s(x, y) = y' = c_5x + c_6y + c_7xy + c_8 \quad (\text{II-5})$$

The eight coefficients, $c_i, i = 1, 2, \dots, 8$, constitute the geometric distortion model used to transform all pixels within the quadrilateral region defined by the tie-points used to obtain the coefficients.

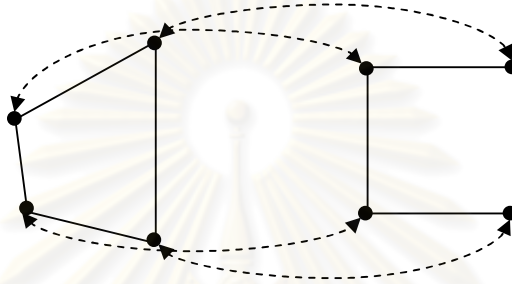


Figure II-3: Corresponding tie-points in two images

2.1.2. Light polarization

A ray of light can be described by its electric field waveform $E(t)$. Different polarization states can be described by decomposing $\vec{E}(t)$ in two mutually orthogonal components $E_x(t)$ and $E_y(t)$ as shown in Figure 2-4. Light becomes linearly polarized light when its two components oscillate in phase or exactly half wavelength in relative phase. Un-polarized light results from the nondeterministic superposition of $E_x(t)$ and $E_y(t)$ [6].

Linearly polarized light can be obtained by passing un-polarized light through a linear polarizer, a filter characterized by the orientation β of the plane in which the electric field is forced to oscillate. If linearly partially polarized light of orientation θ is passed through a linear polarizer of orientation β , the intensity of the resulting polarized light is a function of $(\theta - \beta)$ [12] called the transmitted radiance sinusoid (TRS) and given by equation 2-6 [6].

$$TRS = \frac{I_{max} - I_{min}}{2} + \frac{I_{max} - I_{min}}{2} \cos(2\beta - 2\theta) \quad (\text{II-6})$$

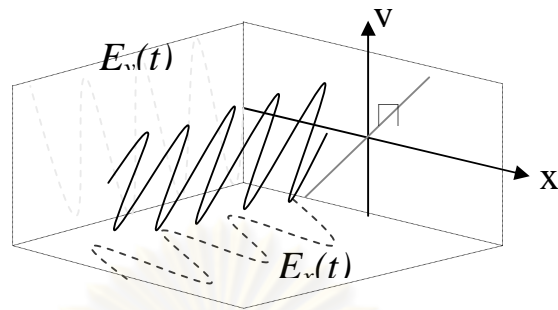


Figure II-4: Two orthogonal components forming the polarization state of the light wave

2.1.3. Iterative Closest Point (ICP) algorithm

Iterative Closest Point algorithm is used for registering digitized data from unfixed rigid objects (P) with an idealized geometric model (X) prior to shape inspection. The algorithm in general is as following [7].

The point set P with N_p points $\{\bar{p}_i\}$ from the data shape and the model shape X (with N_p supporting geometric primitives: points, lines, or triangles) are given.

1. Initial transformation
2. Iterative procedure to converge to local minima

$\forall p \in P$ find closest point $x \in X$

Transform $P_{k+1} \leftarrow Q(P_k)$ to minimize distance between each p and x

Terminate when change in the error falls below present threshold

3. Choose the best among found solutions for different initial positions

2.1.4. Hausdorff distance

Hausdorff distance is defined in [8] as the maximum distance of a set to the nearest point in the other set. In another word, Hausdorff distance from set A to set B can be numerically described as following.

$$h(A, B) = \max_{a \in A} \{ \min_{b \in B} \{ d(a, b) \} \} \quad (\text{II-7})$$

When a and b are points of sets A and B respectively, and $d(a, b)$ is the distance between these points. The algorithm can be described as shown below

1. $h = 0$
2. for every point a_i of A ,

$$\textit{shortest} = \textit{inf}$$

For every point b_j of B

$$d_{ij} = d(a_i, b_j)$$

If $d_{ij} < \textit{shortest}$ then $\textit{shortest} \leftarrow d_{ij}$

If $\textit{shortest} > h$ then $h \leftarrow \textit{shortest}$

2.2. Related works

This section is divided into four parts. The first part is about reviewed works related to laser peak detection methods. The second part is reviewing the range sensors development in the past 20 years and the building of simple 3D scanning in various methods. The third part summarizes some with works aiming to reduce the complexity of the scanning system. The fourth part discusses about some with works related to scanning non-Lambertian surface objects. The fifth part summarized the related work.

2.2.1. Laser peak detection methods

The optical properties of the surface significantly determine the performance of the laser scanner. Totally Lambertian surface with high reflective index is the most proper surface for the scanning because of the noise created by non Lambertian surface. An example is shown in Figure 2-5. Several methods, both computation algorithms [9] and using filter [10], have been proposed to improve the scan line, and consequently the scanning system. Fisher et al. compared five peak detection algorithms in 1991 [9]. The results implemented by the five algorithms were compared in several aspects. In 2004, Forest et al. proposed method to detect the laser stripe using FIR filter approach [10]. The results from the new method gives better estimation of the peak position compared to the results from the five algorithms in [9]. The method however needs a digital filter which consequently increases the cost of the system.



Figure II-5: Laser stripe on (a) Lambertian Surface (b) Translucid

2.2.2. 3D scanner technology

Review of 20 Years of Range Sensor Development by Blais stated that there are 3 main categories of technologies used for developing the noncontact optical surface digitizers; Single point laser scanner, Slit scanner, Pattern projection and Moire and Time-of-Flight system [1]. The practical development of 3-D laser range sensors closely follows the availability of the electronic components and electro-optical emerging technologies. Time-of-Flight scanners are by far the preferred choice for measurements large structures with longer ranges. For the single point laser scanner, the accuracy and the stability of the range data is higher compared to other methods but, at the same time, the cost is higher according to the specialized components and the use of

scanning mechanical devices[1]. The slit scanner is essentially the extension of the single-point laser scanner by allowing the projection of a laser line and simultaneous detection a complete profile of points in a simple video frame. This kind of 3-D scanner is by far the most widely used triangulation-based-3-D laser scanner because of its optical and mechanical simplicity and cost [1]. The speed of the scanning time is enhanced by the introducing of pattern techniques that use multiple stripes or patterns projected simultaneously on the object. This kind of technique give higher scanning speed compared to mechanically scanning and the use of incoherent light reduces speckle noise consequently provides better surface smoothness. However, the smaller depth of focus of the imaging lens results a smaller absolute accuracy than its laser counterparts [1].

2.2.3. Less complex 3D scanner

According to the simplicity of the 3D reconstruction concept, Triangulation-based 3D scanner is a popular technique for building a low-cost system. Many of researches works have been done to omit the pre-calibration process of mechanics needed in Triangulation-based 3D scanner mention in the previous section. The structured-light 3D scanners omit the mechanical scanning process, as required in laser point triangulation or laser stripe, by projecting a sequential pattern of light stripes on the whole scene [1]. Even though the translation stage is not needed for scanning, however, the relative position between light source and camera is still needed to calibrate for depth reconstruction. As same as Bouguet and Perona's work, the method of depth reconstruction is simplified by the presence of a ground plane [11]. The wand is swept in front of the light source which creates a shadow on the surface and the ground plane. The relative depth difference is used for depth computation. In this case, the angle between the plane and the light source has to be known. Fisher, Ashbrook, Robertson and Werghi proposed a way to compute the range differently by tracking the position of the wand itself [12].

Apart from the traditional triangulation concept, there are some works that reduce the complexity of the pre-calibration process by combining the triangulation concept with stereo vision. Davis and Chen proposed a two camera range scanner design that eliminates all actuated components from the calibrated geometry. The two static imagers forming a stereo vision are used to locate a laser stripe as it sweeps over an object. The relative positions between two known viewpoints are

used to compute the depth [13]. In 2009, Aliaga, Zhang and Boutin proposed a pose-free formulation for 3D reconstruction. With the estimation and optimization technique, the system allows to freely taking pictures and moving and un-calibrated digital projector, scene acquisition and scene points reconstruction from few viewpoints [14]. In 2010, Rianmora and Koomsap proposed a method to reconstruct a 3D model using structured-light based method with projective transformation. The homography between the perceived image from a camera view and the stage is obtained by pre-calibration process [15].

2.2.4. Scanning non-Lambertian surface

Reconstructing 3D model using triangulation-based method of non-opaque objects has been always a problem for researchers due to the domination of global illumination effects such as inter-reflection. To acquire a correct range 3D model of such an object, it has been necessary to spray the part with matte paint to suppress inter-reflection. It is not possible to apply this approach in every case especially when the objects need careful handling. There are many researches studying suppressing the global illumination effects in order to obtain a correct depth of the object.

For example, in 1996, Clark et al. used polarization analysis in triangulation-based laser scanning [6] to disambiguate the true laser stripe from spurious inter-reflection on metal surfaces. The assumption was made on the fact that the parameters of linearly polarized light (primarily its orientation) change upon each specular reflection on the metal surfaces. The method is based on the physical properties of reflected light, therefore more general and less dependent on the geometry of the observed surfaces. In their experiment, two linear polarization filters were attached at the light source and the detector. The change in the orientation of the linear polarization was studied to distinguish between single reflections and inter-reflections. Some results from their experiment are shown in Figure 2-6. The experiment was done with few samples mainly metallic objects and did not show the reconstructed 3D model.

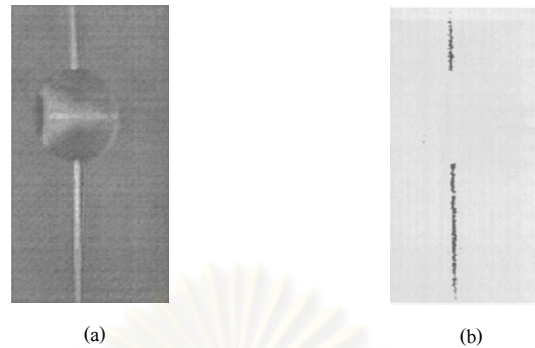


Figure II-6: Experimental result [9] (a) Image of true laser stripe with inter-reflection created by a cylindrical hole in a metal surface (b) Discrimination of true stripe from inter-reflection

Nayar's work was extended by Tongbo Chen et al. in 2007 studying 3D scanning of translucent surface objects [17]. Their research employed Nayar's separation method and Polarization-Difference Imaging (PDI) focusing on reducing subsurface scattering of translucent objects. Translucent objects were projected by structured light while polarization filters were put in front of the projector and the camera. The results show that all the global components were removed using PDI (Figure 2-7(d)). Applying parallel polarization sometimes provides a better Signal-to-Noise Ratio resulting in less noisy range maps (Figure 2-7(c)).

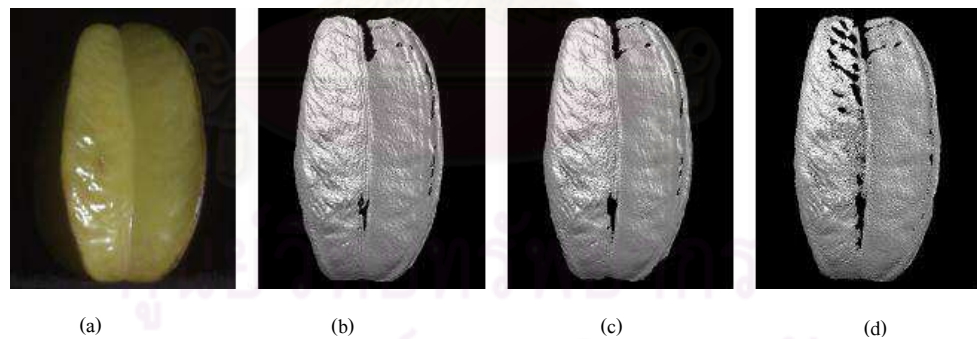


Figure II-7: Experimental result [12] (a) Scene (b) Phase-shifting (c) Parallel polarization (d) PDI

In 2009, Eren et al. proposed a new method to estimate 3D shape of transparent object from local surface heating [18]. The surface of the object is heated by a laser source and the thermal image is acquired then the pixel coordinates are calculated by triangulation. Even the heated surface approach allows the laser line appears on a transparent surface but it is not suitable with careful handling object such as Khon ornaments.

2.2.5. Summary

The goal of this thesis is to formulate a new 3D modeling system that has low cost and less complexity. Moreover, it should be able to scan shiny surfaces. In this section, we briefly review some of laser peak detection methods, well-known 3D scanning techniques, less complexity 3D scanner and techniques to scan non-Lambertian surfaces objects.

Section 2.2.1 reviews the works that are related to the laser peak detection algorithms and technique to improve the laser scan line. Even though employing a digital filter seems to give a better results but the cost of the system would be higher.

The 3D scanning systems based on several techniques are discussed in section 2.2.2. Even though those techniques are the state-of-art and the accuracy of such systems is high, however, the synchronization between mechanical device and complex electronic circuit always rise up the cost of the systems.

The less complexity and low cost 3D scanning systems are discussed in section 2.2.3. The scanning cost is kept low but the knowledge of the relative position between the camera and the light source or fixed cameras' positions are still needed for accurate 3D reconstruction. The errors of the systems are mainly due to the accuracy of the pre-calibration process.

Section 2.2.4 discussed the 3D scanning techniques aiming to solve the scanning non-Lambertian surface objects as mostly found in the ornaments. Using polarization filter to extract the laser peak seems to provide the least complex system.

“In-house 3D Laser Scanner for Khon ornaments”, the title implies about the requirement of the 3D scanning system. The system should be easy to set up and low cost. Moreover, it should be able to reconstruct 3D models of some non-Lambertian surface objects. Next chapter will explain the method to build such system.

Chapter III

3D scanning system

The system proposed here is the best of our knowledge, the first 3D modeling system that purely based on image processing. This consists of 3 sections: overview of 3D scanning system, the 3D laser scanner design and the algorithms and data.

3.1. Overview of 3D scanning system

The 3D scanners available for commercial use nowadays are expensive (~\$3000) [19] due to the cost of production [1]. Some researchers have focused on building low-cost 3D scanning system by reducing the complexity of the setup [1,11-14, 20]. However, those systems were implemented from the triangulation concept which the correspondence locations between light source, camera and surface of the object have to be known. The goal of this thesis is to design and implement a 3D scanning system that is easy to set up, low cost and able to reconstruct 3D models. The thesis also studies about using light polarization effect to solve the problem of scanning non-Lambertian surfaces objects.

The method proposed here reduced the complexity and the cost of the system by formulating a new way of a 3D modeling scheme that does not depend on the correspondence between the camera, object and light source. The proposed method is purely based on a digital image processing concept, so called “geometric transformation”. By knowing the “tie-points”, the pixels inside the quadrilateral area is likely to be recovered. This can be done through a special design box that can give us the information of the “tie-points” to construct the transformation matrix of each frame. Those are essentially needed for 3D computation. The process of reconstructing 3D point cloud is shown in Figure 3-1. The system proposed in this thesis is divided into 2 parts: the 3D laser scanner design and the data analysis.

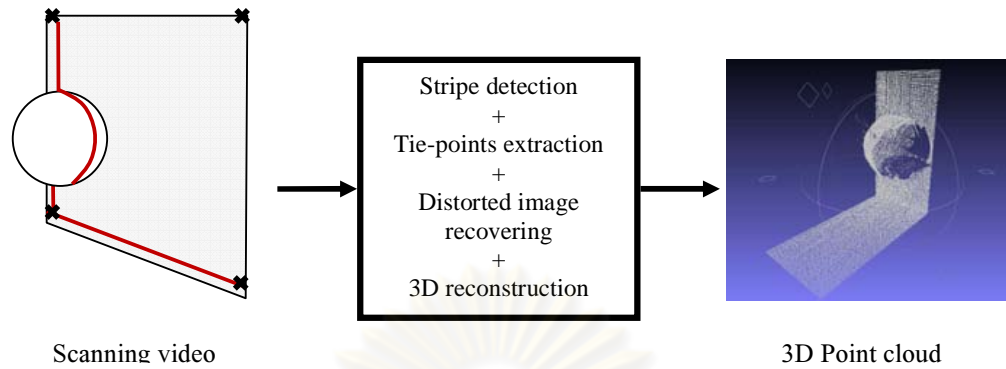


Figure III-1: Process of recovering the distorted image

3.2. 3D laser scanner design

The key points of designing the 3D laser scanner are detecting the laser stripe reflected from the surface and constructing the transformation matrix using tie-points. The proposed 3D scanner consists of five main components as shown in Figure 3-2 which are laser source, cylindrical lens, translation stage, camera and pre-designed reference box. The cylindrical lens that is located in front of the laser source in order to create a laser stripe. The laser stripe will be projected on an object that is situated in a reference box. The speed and the direction of the translation are controlled by the circuit board situated in a box. The reference box was build from two orthogonal planes and a string. The tested objects are sphere, rectangular box, cylinder, cone and orthogonal planes. The laser stripe will be projected across the object by the translation stage. The deformation of the laser stripe with respect to the shape of the object is recorded by a camera. The images should be captured in the way that the four corners (tie-points) of the area of interest should be seen by the camera as shown in Figure 3-3. This region is analyzed as described in the next section.

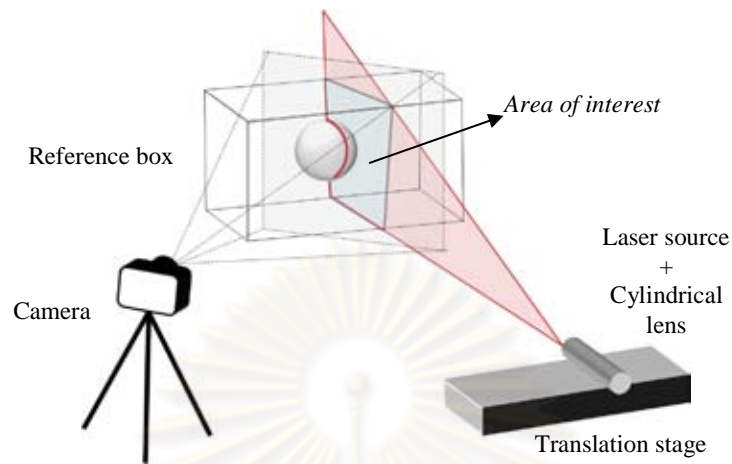


Figure III-2: Conceptual 3D Laser Scanner

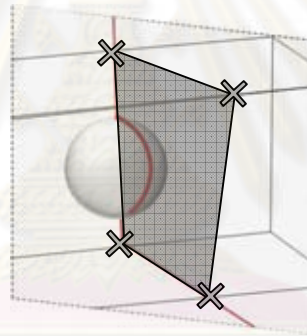


Figure III-3: Captured images with the presenting of tie-points

3.3. Algorithm and data

This section shows the process of 3D point cloud reconstruction. It consists of four main steps which are data acquisition, image processing, 3D reconstruction and registration. The algorithms of each step are explained as following.

3.3.1. Data acquisition

The video is extracted and assigned the name to each extracted frames. The algorithm is designed to perform the computation in each frame, hence eliminating the need of pre-calibration process

to obtain the camera parameters and correspondence location of the camera and the light source. The extracted frames (n frames) are kept in an array as shown in equation 3-1.

$$F = \{frame_1, frame_2, \dots, frame_n\} \quad (III-1)$$

When every elements in F is 3-dimensional matrices as described below

$$frame_i = [size_x, size_y, colors] \quad (III-2)$$

The first two elements of $frame_i$ represent the size of the images (s_x, s_y). The third element represents the data in three color domains which are *red*, *green* and *blue*. Figure 3-4 visually shows the data contained in each $frame_i$.

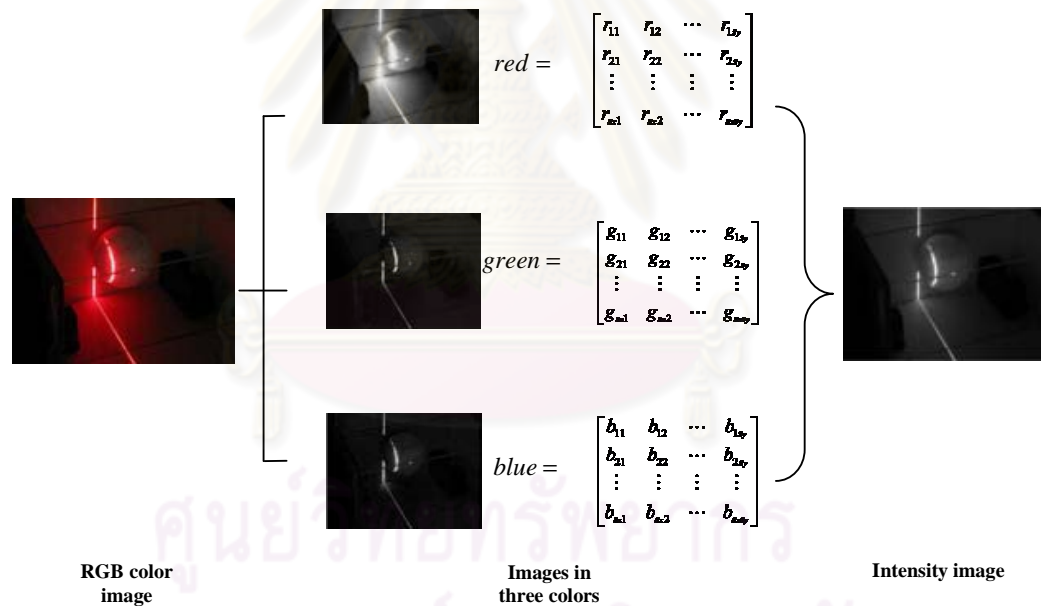


Figure III-4: Converting RGB color image to intensity image

3.3.2. Image Processing

In this process, four major steps are performed: reference lines defining, peak finding, tie-points finding and fixing distortion. The algorithms of each process are explained below.

3.3.2.1. Reference line defining

The sets of points described the reference lines are essentially needed for 3D computation. The algorithm of reference lines defining is shown in Figure 3-5.

- 1 Display $frame_1$
- 2 Change the color domain (RGB) of the $frame_1$ to intensity domain (grayscale)
3. Assign $P_{11}(x, y)$ and $P_{12}(x, y)$ be a set of points that define a line L_1 by the user
- 4 Construct a set of poi($p_1^1, p_2^1, \dots, p_{sy}^1$) that define L_1
- 5 Assign $P_{21}(x, y)$ and $P_{22}(x, y)$ be a set of points that define a line L_2 by the user
- 6 Construct a set of points ($p_1^2, p_2^2, \dots, p_{sy}^2$) that define L_2
- 7 Assign $P_{31}(x, y)$ and $P_{32}(x, y)$ be a set of points that define a line L_3 by the user
- 8 Construct a set of points ($p_1^3, p_2^3, \dots, p_{sy}^3$) that define L_3
- 9 Assign $P_{41}(x, y)$ and $P_{42}(x, y)$ be a set of points that define a line L_4 by the user
- 10 Construct a set of points ($p_1^4, p_2^4, \dots, p_{sy}^4$) that define L_4

Figure III-5: Algorithm of reference lines defining

This results in four sets of points that are used for defining the edges of the reference box (four straight lines) as shown in Figure 3-6. Those are used for computing the 3D points.

3.3.2.2. Peak finding, tie-points finding and fixing distortion

In these step, the algorithm is perform in each extracted frame in order to find the interested points (the laser line) and to compute the 3D coordinates of those interested points using the tie-points (t_1, \dots, t_d) as shown in Figure 3-6. The extracted frames are first converted to intensity field as shown in Figure 3-4. The algorithm of the process is shown in Figure 3-7 (1-6).

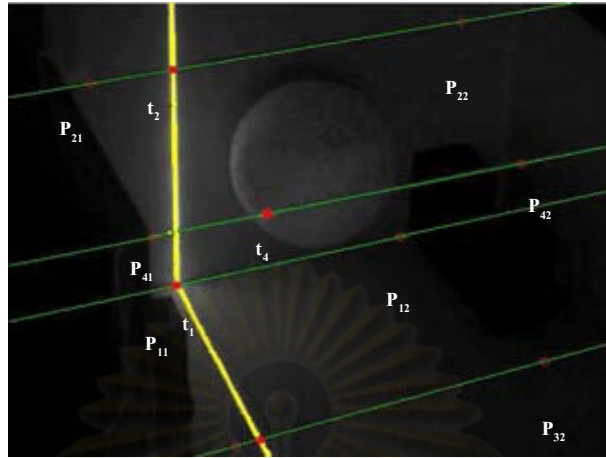


Figure III-6: Parameters defining

- 1 Repeat until $i = n$
- 2 Change the color domain (RGB) of the $frame_i$ to intensity domain (grayscale)
- 3 Assign S be the set of points $(s_1, s_2, \dots, s_{s_x})$ that store the location of the pixels that have the maximum values of every row
- 4 Assign T be the set of tie-points (t_1, t_2, t_3, t_4) which pick from the values in S that match with the values stored in L_1, \dots, L_4 . These four points are defined as the corners of the reference window (in the experiment is $10\text{cm} \times 10\text{cm}$ window)
- 5 Compute the eight parameters (c_1, c_2, \dots, c_8) by mapping t_1, t_2, t_3 and t_4 to the real world coordinates $[(0,0), (10,0), (10,10), (0,10)]$ solved by the equation
- 6 Assign S' be the set of points $(s'_1, s'_2, \dots, s'_{s_x})$ that store the mapping points solved by the equation 4 and 5
- 7 Compute the space between each frame: $dz \leftarrow \frac{d}{s \times f}$
- 8 Assign the value of z-coordinate to every elements in S' : $S'(z) \leftarrow i \times dz$

Figure III-7: Algorithm of image processing in each frame for 3D modeling

This results in a set of points (S') in x and y coordinates. Next step is to compute the value in z coordinate.

3.3.3.3D reconstruction

The values of the z-coordinate of each frame are computed from the speed of the translation of the laser line at a certain distance. The video is captured at f frames per second while the line travels at the velocity of $\frac{d}{s}$ centimeters per second. It means that the spacing between each frame is $\frac{d}{s \times f}$ centimeters per frame. The algorithm of this process is shown in Figure 3-7 (7-8).

By the end of this process, those interested points in S' contain data in world 3D coordinates. In order to visualize those numerical data, they are stored in a text file and stacked over for every elements in S' . Figure 3-8 shows the point cloud of the scan



Figure III-8: 3D point cloud presented by Meshlab [22]

3.3.4. Registration

In order to reconstruct a complete model, the object has to be scanned several times at different angles. The several scans are then merged together in the registration process. The golden standard method for registration is Iterative Closest Points algorithms described in Chapter 2 [21]. The rough alignment of two sets of point cloud is registered by running the algorithm multiples times by sampling the space of initial conditions. The rough alignment can be done manually or by the use of characteristic markers in the scene. From the experiment, the non-objects point cloud are chosen and deleted manually. Figure 3-9 shows the polished scans that are aligned manually and refined by ICP algorithm provided by open source, MeshLab [22].

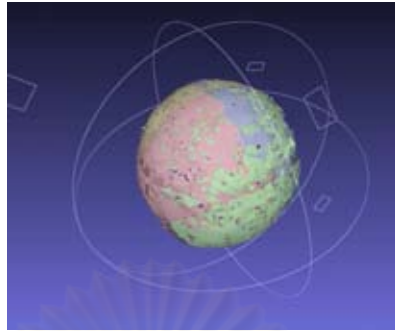


Figure III-9: Point cloud registration



ศูนย์วิทยทรัพยากร
จุฬาลงกรณ์มหาวิทยาลัย

Chapter IV

Experimental results and discussion

4.1. Overview of the experiments

The aim of the proposed 3D reconstruction technique is to reduce the complexity of the 3D modeling system which, consequently, reduces the cost. The conceptual system built on the ‘less complexity and low cost’ is explained in the last chapter. Also, the light polarization concept is studied and applied to the proposed 3D laser scanner for scanning non-Lambertian surfaces. This chapter explains how the experiments were conducted, experimental results and the analysis of the performance and the limitation of the system by performing four experiments. The first experiment is to see how the accuracy of the 3D reconstruction method using linear transformation matrix is limited by distance and angle. The second experiment is to analyze how the accuracy of method is limited by the number of scans and alignment process by doing the experiment on primitive models. The third experiment is to measure the time to make a complete 3D model. The last experiment is to see the characteristic of the reflected light from non-Lambertian surfaces when a linear polarizer is applied in front of the camera. The last section is the discussion of the experimental results from four experiments.

4.2. Measurement of the accuracy of recovering the original points

The objective of this experiment is to test whether the proposed method can correctly recover images from the distorted image using transformation matrix at a certain distance. The transformation matrix is constructed under the assumption that the taken image is linearly distorted. The lens distortion which forms a non-linear transformation is not accounted in this experiment.

4.2.1. Notation

Tie-points define as the pixel points in the distorted image for which the real world coordinates are known [4]

Quadrilateral area is the area that has four sides connected by the four *tie-points* [4]

Transformation matrix is a matrix that consists of eight coefficients corresponding to transform the distorted image to the original image [4]

(A,B) , in this experiment, is the configuration of the checkerboard according to the camera view. A represents the angle (in degree) of the checkerboard tilted according to the vertical axis. B represents the angle (in degree) of the checkerboard tilted according to the horizontal axis. The negative value of A or B means that the checkerboard is rotated clockwise and vice versa.

4.2.2. Task

The experiment was designed to find the optimal configuration of the experimental set up. The marked points inside the quadrilateral area are recovered by linear transformation matrix corresponded to the area. There are six set of images, Case1 to Case6, with four images per set that were tested in this experiment. The configuration of each case and the tested images can be found in Appendix A. In each set, four images were taken by a camera at a certain angle. At one angle, four images are taken at difference distances ranging from 30cm to 75 cm. The size of the images is 448×336 resolution. During doing the experiment, the user will be asked to located thirty six points on the grid. The locations of the points in x-axis and y-axis are compared with the real data and calculated to find the percent of the absolute error.

4.2.3. Equipments

Camera, checkerboard (1inch × 1inch spacing) and tape rule

4.2.4. Hypothesis

The points are reconstructed more accurately when the distortion is linear.

4.2.5. Variables

The variables used in this experiment is explained as shown in Table IV-1

Independent variables	Distance between camera and the checkerboard, marked points on the grid
Dependent variables	Location of the recovered points on the grid
Controlled variables	Size of the checkerboard, Size of the grid, Angle of the checkerboard

Table IV-1:Variables of the experiment one

4.2.6. Procedures

1. Take images at four different distances at an angle. Repeat this step with another six different angles. Total tested images are twenty four. The sample of the four images taken at different distance is shown in Figure 4-1.
2. Choose the image to test
3. Input the information about the size of the checkerboard
4. Choose four tie-points corresponding to the four corners of the checkerboard
5. Mark the points on the grid at the selected quadrilateral area. Starting from bottom to top and left to right. The total number of marked points is thirty six
6. Compare the recovered values with the real data and calculate the average error of the absolute distance.
7. Plot the percent error versus the distances
8. Repeat step 2 to 6 with another three images in the set. Also repeat the steps with another five sets of images

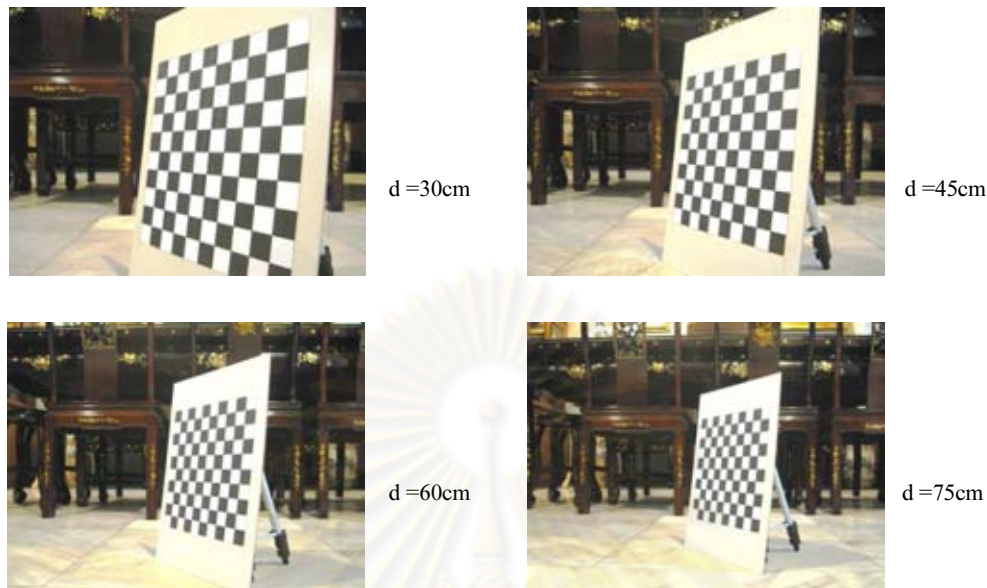


Figure IV-1: Images (-45 degree tilted in z-axis) taken at four different distances

4.2.7. Experimental results

The percent error of each images were calculated by the following. In each image, the thirty six offset values between the real data and the recovered values in both horizontal axis and vertical axis were calculated. The absolute error is calculated by finding the absolute distances of the thirty six offset values. Later, those values were averaged to give the percent error of absolute distance of the image. The x-axis in the graph represents the different distances and the y-axis represents the percent error rates.

Figure 4-2 shows the graph of the percent error of the absolute distances. The average of the error of Case1 is 3.36%. The average of the error of Case2 is 8.68%. The average of the error of Case3 is 12.31%. The average of the error of Case4 is 12.16%. The average of the error of Case5 is 12.53%. The average of the error of Case6 is 15.49%. The case that gives the minimum of averaged error is Case1. The case that gives the maximum of averaged error is Case6. The percent errors of every cases decrease as the distances increase. The images that give the best case, the average case and the worst case are shown in Figure 4-3. The error of Case1 starts to increase as the distance is beyond 45 cm.

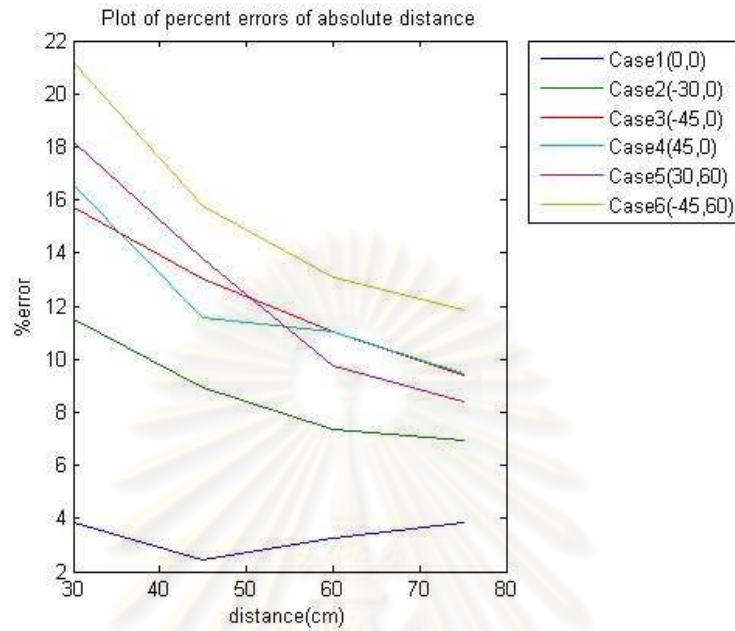


Figure IV-2: The graph presenting percent error of absolute distance and the distance

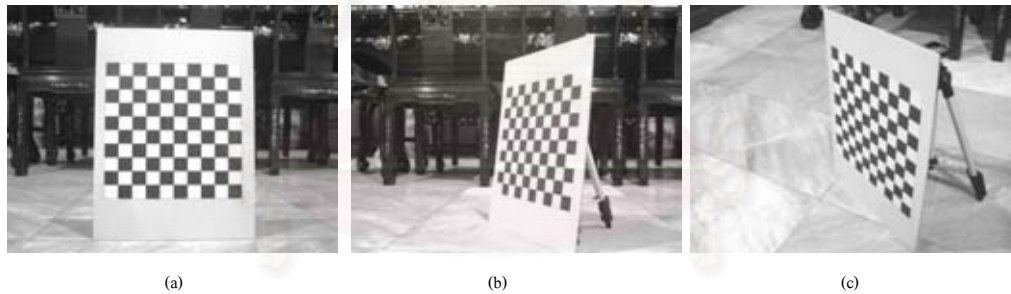


Figure IV-3: The configuration of the scene captured by a camera ($d=60\text{cm}$) (a) best case (b) average case (c) worst case

4.3. Measurement of the accuracy of 3D reconstruction on primitive models

The objective of this experiment is to test the accuracy of the reconstructed 3D primitive models using the proposed scanning method.

4.3.1. Notation

Primitives are the building blocks of 3D-basic geometric that can be used or modified with transforms and Booleans. The most common 3D primitives are cubes, pyramids, cones, spheres and tori [23]

Hausdorff distance is defined in as the maximum distance of a set to the nearest point in the other set [8].

Iterative Closest Point (ICP) algorithm is used for registering digitized data from unfixed rigid objects (P) with an idealized geometric model (X) prior to shape inspection [21].

Audio Video Interleave (AVI) is a special case of Resource Interchange File Format (RIFF) defined by Microsoft. It is the most common format for audio and video [25].

JPEG is a one of the most popular and comprehensive continuous tone, still frame compression standards [4]

American Standard Code for Information Interchange (ASC or ASCII) is a text standard that consists of 128 characters (0-127) covering alphabetical, numerical, punctuation, and a few text control characters [24].

4.3.2. Task

The experiment was designed to measure the accuracy of the reconstructed 3D models using the 3D laser scanning system proposed in this thesis. There are five primitive models tested in this experiment: sphere, rectangular box, cylinder, cone and orthogonal planes. The configuration of the set up is not fixed. However, the scanning region must not face the lens distortion effect. The scans at different view of each model are registered manually and then refined with ICP algorithm. The reconstructed 3D models are compared with the computer generated 3D models to measure the RMS error using Hausdorff distance.

4.3.3. Equipments

The proposed 3D laser scanner built from the conceptual design in Chapter 3. The images of the real experimental setup and equipments are shown in Appendix B. The images of the tested objects are shown in Appendix C.

4.3.4. Hypothesis

The numbers of the scans needed for reconstructing a 3D models and registering process affect the error rate

4.3.5. Variables

The variables used in this experiment are explained as shown in Table IV-2

Independent variables	Number of scans and registering those scans
Dependent variables	RMS error rate
Controlled variables	The tested models, the parameters of the set up (angle, distance)

Table IV-2 Variables of experiment two

4.3.6. Procedures

1. Record a video (.avi) while the objects is scanned using the proposed 3D laser scanner
2. Extract the image frames (.jpeg) from the video
3. Store the extracted frames in a folder
4. Process the extracted frames by running the program
5. Follow the instruction of the program
6. Open the export file (.asc) using Meshlab

7. Manually perform the post-processing by discarding the outlier vertices and registering the scans

8) Record new video of scanning the object at different angle and perform 1) to 7) if needed

4.3.7. Experimental results

The results of the experiment two are shown in Table IV-3. The first column shows five different types of the tested objects. The dimensions of those are shown in the second column. The numbers of scans to form a complete 3D model are shown in the third column. The minimum offset values are shown in the fourth column. The maximum offset values are shown in the fifth column. The RMS errors are shown in the last column. The unit of the values in the last three columns is centimeter.

Objects	Dimensions	No. of scans	Min. Offset	Max. Offset	RMS error
Sphere	4cm. diameter	5	0.0000	0.2138	0.0392
Rectangular box	5.9cm×5.9cm×2cm	5	0.0000	0.3098	0.0575
Cylinder	1.75 radius with 3cm height	4	0.0000	0.1211	0.0236
Cone	1.6 radius with 4cm height	5	0.0000	0.1603	0.0524
Planes	10cm×10cm	1	0.0000	0.1137	0.0010

Table IV-3: Results of the experiment two

The results shows that the orthogonal plane, which requires only one scan and does not need to perform the alignment process, gives the lowest RMS error. The models that require more number of scans and have to do the alignment process give higher RMS error. Figure 4-4 shows the reconstructed models of the best case (orthogonal plane), the average case (cylinder) and the worst case (rectangular box). The colorized point cloud represent the error distance compared

with the computer generated models. Red color represents low error distance while the green color represents the high error distance.

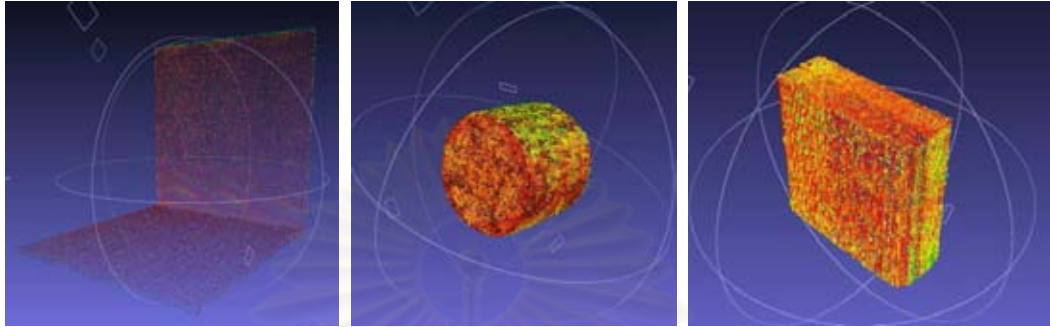


Figure IV-4: The colorized 3D reconstructed models (a) the best case (b) the average case (c) the worst case

4.4. Measurement of time spent on reconstructing a complete 3D model

The objective of this experiment is to examine the time used to reconstruct a complete 3D model.

4.4.1. Notation

Scan time is time to scan an object at a certain distance. In this experiment, the distance is set to 10 cm and the scanning time is set to 23 seconds

Processing time is the time to process the video and reconstruct the 3D point cloud

Alignment time is the time spent on registering the several scans manually

4.4.2. Task

The time used for making a complete 3D model can be divided into three parts: scanning time, processing time and scan alignment time. This experiment was designed to examine the time spent on each part. The extracted frames from the video have 640×480 resolution

4.4.3. Equipments

Same as 4.3.3

4.4.4. Hypothesis

Under the constraints of the testing environment, the resolution of the images and scanning time, the time spent on completing a 3D model varies proportional with the number of scans.

4.4.5. Variables

The variables used in this experiment is explained as shown in Table IV-4

Independent variables	Number of scans, time spent on alignment process
Dependent variables	Time to reconstruct a complete 3D model
Controlled variables	The tested models, the testing environment (computer system), the parameters of the set up (angle, distance), the resolution of the images, scanning time

Table IV-4 Variables of experiment three

4.4.6. Procedures

1. Record the video of scanning an object. The time the light is swept on the object at a distance of 10cm is 23 seconds.
2. Perform the 3D reconstruction using the program with the video.
3. Measure the time for finishing the process.

4.4.7. Experimental results

Table IV-5 Time to reconstruct complete 3D models and Figure IV-5 shows the time needed in each process to finish reconstructing 3D models. The speed of the processing time running on the system of Intel® Core™ i5 CPU with 4GB of memory is 1-2 frames per second. The x-axis represents different kind of objects that are used in the experiment. The y-axis represents the time used for completing a 3D model. Each bar consists of 3 different colors. White color represents the time used for scanning the object. Red color represents the time used for 3D reconstructing

process. Blue color represents the time used for the aligning process. The three period of time are stacked over one another to give the total.

The model that used the least time to complete is the orthogonal plane that does not require the alignment process. And it requires much time to complete reconstructing the paper cup model which has the highest number of scans.

Objects	Number of scans	Estimation of scanning time (min)	Estimation of processing time (min)	Estimation of Total time (min)
Sphere	5	2	21.25	23
Rectangular box	5	2	21.25	23
Cylinder	4	2	17	19
Cone	5	2	21.25	23
Orthogonal planes	1	0	4.25	5
Paper cup	8	3	34	37
Toy	6	2	25.5	28

Table IV-5 Time to reconstruct complete 3D models

ศูนย์วิทยทรัพยากร
จุฬาลงกรณ์มหาวิทยาลัย

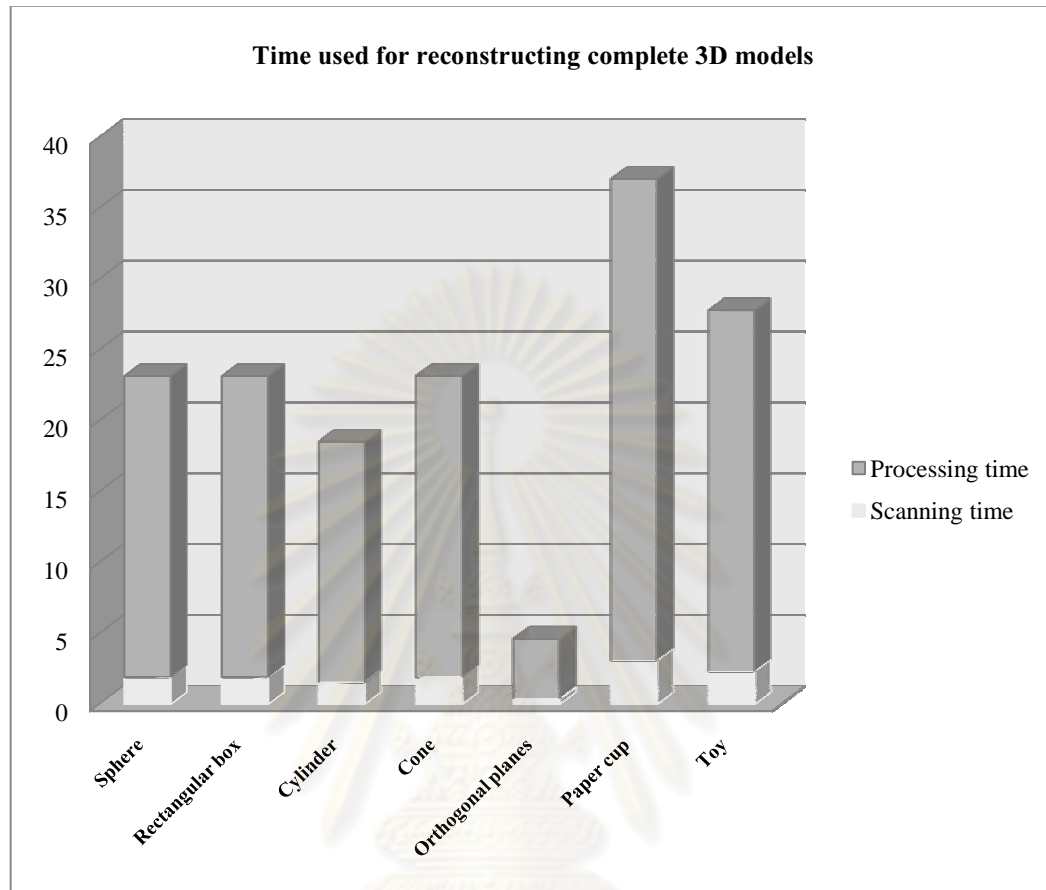


Figure IV-5: The chart represents the time spent on reconstructing complete 3D models

4.5. Comparing the effect of applying linear polarizer on the light characteristic when reflected on non-Lambertian surfaces

The objective of this experiment is to examine the effect of using linear polarizer when the laser light is shone on non-Lambertian surfaces.

4.5.1. Notation

Lambertian surface is the surface point that can be assumed to have a similar color in images taken from different view-points. The light is diffused on the surface [25]

Non-Lambertian surfaces is the surface point that cannot be assumed to have a similar color in images taken from different view-points. The light is partly diffused or reflected on the surface [25]

4.5.2. Task

This experiment was designed to see the light characteristic when the stripe of light is shone on non-Lambertian surfaces and the light when the linear polarizer is put in front of the camera. There are two types of material tested in this experiment. The surfaces of the tested material are opaque and give non-ideal specular reflectance. The laser stripe is shone on the surfaces and captured by a camera. Two images (with 90 degree orientation linear polarizer and with 180 degree orientation linear polarizer) are taken and subtracted the intensity to see the effect.

4.5.3. Equipments

Objects, linear polarizer and camera

4.5.4. Hypothesis

The polarization state of the light after reflected from a surface is preserved if the surface is non-Lambertian.

4.5.5. Variables

The variables used in this experiment is explained as shown in Table IV-6

Independent variables	The image taken with 90 degree and 180 degree orientation of linear polarizer
Dependent variables	The observed images
Controlled variables	The tested non-Lambertian surfaces, the parameters of the set up (angle, distance)

Table IV-6: Variables of experiment four

4.5.6. Procedures

1. Finding the polarization state of the laser light. This step can be done by putting the linear polarizer in front of the laser source, adjust the angle of the polarizer until the laser light disappears (it means that the polarization state of the laser source and the polarizer is perpendicular or 90 degree)
2. Take the image of the laser strip that shone on the surface
3. Turn the angle of the polarizer 90 degree (this degree of the polarizer is the same as the polarization state of the laser or 180 degree)
4. Capture the image of the laser strip that shone on the surface
5. Subtract the intensity of the image taken at 180 degree orientation with image taken at 90 degree orientation. Observe the subtracted image

4.5.7. Experimental results

Table IV-7 shows the experimental results. The first column of the table shows the type of material. The second column shows the images taken at 180 degree polarizer equipped in front of the camera. The intensity of the light that scattered from the surfaces is strong. The third column shows the images taken with 90 degree polarizer equipped in front of the camera. The intensity of the images is diminished especially on the surfaces which is non-Lambertian. The fourth column shows the subtracted images. The experimental results show that most of intensity of the light on the Lambertian surface (the two orthogonal planes) is mostly eliminated in the subtracted images. The intensity of the light on non-Lambertian surfaces (the tested objects) is visible.

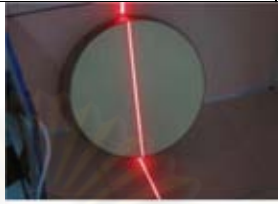
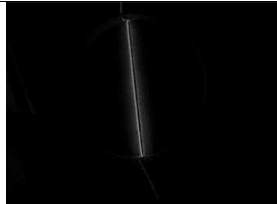
Type of surfaces	Images taken with 180 deg linear polarizer (A)	Images taken with 90 deg linear polarizer (B)	The subtracted images (C=A-B)
Galvanized iron			
Silver			

Table IV-7: Images taken at different orientation of polarizer and subtracted images

4.6. Discussion

In this section, the performance of the proposed 3D modeling method prepared for scanning real world objects and some Khon ornaments is discussed in several aspects. First, the accuracy of the reconstructed 3D models is limited by the distance and the angle between the captured scene and camera, the number of scans and the alignment process and the resolution of the camera as shown in the first and the second experiment. Second, the time to reconstruct complete 3D models mainly depends on the number of scans as shown in the third experiment. Third, the use of linear polarizer is a possible way to distinguish the light that scattered from non-Lambertian surfaces. The discussions on each experiment are explained as following.

The results from the first experiment show that the accuracy of the recovering method using linear transformation can be enhanced if the configuration of the camera and the captured quadrilateral area is optimal. Percent error of the recovered data is reduced when the area is captured at a large distance (more than 60cm from the experiment). This is because the lens distortion, which creates non-linear transformation, does not have an effect on the scene. The angle between the quadrilateral area and the camera also affects the accuracy of the method. The best case is when the area is captured without any tilting. However, the error increases when the

image is captured at the distance beyond 45cm. This might be because the image is too small so that the grid is not marked by the user correctly. The average case is when the area is tilted by 30-45 degree. The worst case is when the area is tilted by more than 60 degree. However, it is noticeable that the percent error of the area that is tilted by 60 degree also gives the average percent error (at the distance over 60cm) as shown in graph in Figure 4-2. As the points were marked manually, the percent error of many cases might be mainly due to the human error.

The accuracy of the 3D reconstructed models is also affected by the number of scans, the aligning process. This is shown in the second experiment where the model that has the minimum error required only one scanning and did not need to perform the manually alignment. The accuracy of the system can be enhanced by developing automatic alignment tool or finding the way to reconstruct a complete model using the least number of scans. Also, the tested objects are not measured precisely by standard calibration tools which may affect the error rate when comparing the scanned 3D models with the computer generated ones.

The time that is spent on reconstructing complete 3D models mainly relied on the 3D processing and the alignment process which is done manually. The speed of reconstructing a complete model can be enhanced by using automatic point cloud alignment tool. Also the algorithm for the 3D reconstruction can be revised and developed to increase the speed.

The fourth experiment shows the results of applying linear polarizer for scanning non-Lambertian surfaces. Two images, one taken with linear polarizer which the orientation is set at 180 degree and one with the orientation is set at 90 degree, are compared to see the effect. When the images were taken with 180 degree orientation of polarizer, the intensity on non-Lambertian surfaces (the object surface) and Lambertian surfaces (paper) is strong. However, it is noticeable that the intensity of the light on is diminished on non-Lambertian surfaces when the images were taken at 90 degree polarizer while the intensity of the light on Lambertian surfaces remains the same. This is because the polarization state of the light when scattered out from Lambertian surfaces (such as paper) is randomly polarized. There is high probability that the polarization of the light is matched with the orientation of the polarizer. However, the light that scattered from non-Lambertian surfaces still partly preserves its polarization state. The idea to extract the line on non-

Lambertian surfaces is by subtracting two images taken at different polarization. The experimental results show that this technique is one possible way to distinguish the light that scattered out from non-Lambertian surface. This can be applied with the proposed 3D laser scanning system for scanning reflective surface which is mostly found in ornaments.



ศูนย์วิจัยทรัพยากร
จุฬาลงกรณ์มหาวิทยาลัย

Chapter V

Conclusion and future work

This chapter consists of two sections. The first section concludes the overall of the thesis and provides some discussion on the experimental results. The second section suggests the future development that can be extended.

5.1. Conclusion

This research presents a new method to build a low cost and less complex 3D modeling system that will be used for collecting digital data of real world objects. The study of using light polarization concept to reduce the problem of scanning non-Lambertian surfaces was also carried. The 3D modeling system proposed in this thesis consists of two parts: the 3D laser scanner and the software. The cost and the complexity of the 3D laser scanner are reduced by the pre-fabricated reference box. The advantage of applying the reference box is to eliminate the pre-calibration process of finding the correspondence relation between the camera and the light source; hence, the camera can be freely moved. This is a new method of reconstructing a 3D model using 3D laser scanner. The software that works with the proposed 3D laser scanner is implemented and the algorithm of 3D model reconstruction is also presented in this thesis. The experimental results show that the accuracy of the 3D reconstruction method depends on many factors. The first factor is the distance and the angle between the camera and the reference box. The percent error of the recovered data decreases when the distance increases. This is because the quadrilateral area is linearly distorted looking from a camera. The second factor is the number of scans that are needed to be registered. This is because the registering process is done manually. The more the number of scans, the more human error gets involved. The third factor is the resolution of the camera. The larger the resolution of the images means the higher chance that the laser peak is correctly chosen and consequently the more accurate the 3D reconstructed models is. The study of light polarization on different surfaces shows that it is possible to distinguish the light that scattered from Lambertian and non-Lambertian surfaces using linear polarizer. However, two images are required.

5.2. Future works

There are many rooms for developing the 3D modeling system proposed in this thesis. First, the optimal configuration of the set up can be tested and improved. The cost of the scanner could be reduced by substituting some of the equipments with a low cost one. Second, new design of the algorithm for 3D reconstruction can be further developed to increase the speed of the software. Third, more experiments and further study to validate the concept of using light polarization to help scanning non-Lambertian surfaces is needed.

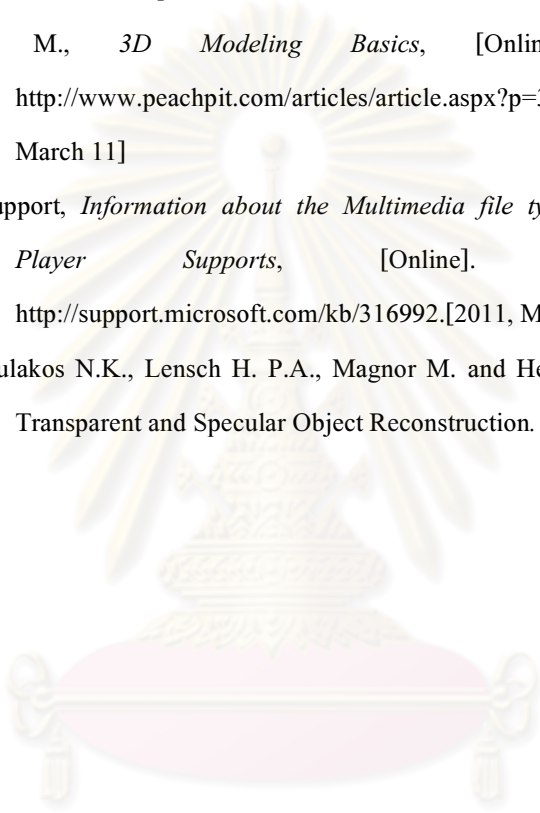


References

- [1] Blais, F., Review of 20 years of range sensor development. *Journal of Electronic Imaging* 13 (2004): 231-240
- [2] Lanman, D., and Taubin, G., Build your own 3D scanner: 3D photography for beginners. *ACM SIGGRAPH 2009 Courses*, p.1-94, August 03-07, New Orleans, Louisiana, 2009
- [3] Davis, J., and Chen, X., A laser range scanner designed for minimum calibration complexity. *Third International Conference on 3-D Digital Imaging and Modeling* (2001): 91-98
- [4] Gonzalez, R. C., and Woods, R. E., *Digital Image Processing*, Prentice Hall, 2001.
- [5] *Mathworks*, [Online]. Available from: <http://www.mathworks.com/help/toolbox/images/ref/rgb2gray.html> [2011, February 20]
- [6] Clark, J., Trucco, E., and Wolff, L. B., Using Light Polarization in Laser Scanning. *Image and Vision Computing* 15 (1997): 107-117
- [7] Besl, P. J., and McKay, N. D., A Method for Registration of 3-D Shapes. *IEEE Transactions on Pattern Analysis and Machine Intelligence*, 14, 2 (February 1992): 239-256
- [8] Grégoire, N., and Bouillot, M., *CS 507 Computational Geometry McGill University*, [Online]. Available from: <http://www-cgrl.cs.mcgill.ca/~godfried/teaching/cg-projects/98/normand/main.html> [2011, February 20]
- [9] Fisher, R. B., and Naidu, D. K., A Comparison of Algorithms for Subpixel Peak Detection. *Image Technology, Advances in Image Processing, Multimedia and Machine Vision* (1996): 385-404
- [10] Forest, J., Salvi, J., Cabruja, E., and Pous, C., Laser stripe peak detector for 3D scanners. A filter approach. In *Proceedings of the Pattern Recognition (ICPR) , 17th International Conference on (ICPR)* (2004): 646-649

- [11] Bouguet, J. Y., and Perona, P., 3D photography on your desk. *Sixth IEEE International Conference on Computer Vision*, Narosa Publishing House, New Delhi, India, 1998.
- [12] Fisher, R. B., Ashbrook, A. P., Robertson, C., and Werghi, N., A low-cost range finder using a visually located, structured light source. *Second International Conference on 3-D Digital Imaging and Modeling*, IEEE Comput. Soc, Los Alamitos, CA, USA, 1999.
- [13] Davis, J., and Chen, X., A laser range scanner designed for minimum calibration complexity. *Third International Conference on 3-D Digital Imaging and Modeling* (2001): 91-98
- [14] Aliaga, D. G., Zhang, J., and Boutin, M., A Framework for Modeling 3D scenes using Pose-free Equations. *ACM Transactions on Graphics*, (29), 2009
- [15] S. Rianmora and P. Koomsap, Applying 2D Projective Transformations for Structured Light System-Based Selective Data Acquisition. *The 2nd International Conference on Computer and Automation Engineering (ICAAE)* (2010)
- [16] Nayar, S. K., Krishnan, G., Grossberg, M. D., and Raskar, R., Fast separation of direct and global components of a scene using high frequency illumination. *In proceedings of IEEE International Conference on Computer Vision (ICCV)* (2005): 420-427
- [17] Chen, T., Lensch, H. P. A., Fuchs, C., and Seidel, H.-P., Polarization and Phase-Shifting for 3D scanning of Translucent Objects. *In proceedings of IEEE Computer Society Conference on Computer Vision and Pattern Recognition (CVPR)* (2007): 1-8
- [18] Eren, G., et al., Scanning from heating: 3D shape estimation of transparent objects from local surface heating. *Optics Express*, 17, 14 (2009): 11457-11468
- [19] *NextEngine, The #1 Selling 3D Scanner*, [Online]. Available from: <https://www.nextengine.com/> [2011, February 20]
- [20] *DAVID laser scanner*, [Online]. Available from: <http://www.david-laserscanner.com/> [2011, February 20]

- [21] Makadia, A., Patterson IV, A., and Daniilidis, K., Fully Automatic Registration of Multiple 3D Data Sets. *Image and Vision Computing*, 21 (2001): 637-650
- [22] Visual Computing Lab of Istituto di Scienza e Technologie dell'Informazione "A. Faedo". *Meshlab*. [Online]. Available from: <http://meshlab.sourceforge.net> [2010, December 11]
- [23] Giambruno, M., *3D Modeling Basics*, [Online]. Available from: <http://www.peachpit.com/articles/article.aspx?p=30594&seqNum=5> [2011, March 11]
- [24] Microsoft Support, *Information about the Multimedia file types that Windows Media Player Supports*, [Online]. Available from: <http://support.microsoft.com/kb/316992>. [2011, March 11]
- [25] Ihrke I., Kutulakos N.K., Lensch H. P.A., Magnor M. and Heidrich W., State of Art in Transparent and Specular Object Reconstruction. *EUROGRAPHS*, 2008.



ศูนย์วิทยทรัพยากร
จุฬาลงกรณ์มหาวิทยาลัย



APPENDICES

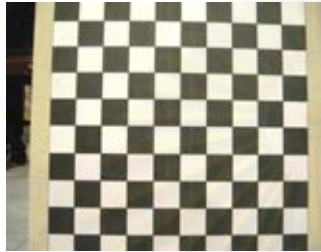
ศูนย์วิทยทรัพยากร
จุฬาลงกรณ์มหาวิทยาลัย

APPENDIX A

This section shows the images sets that were used in experiment 1.

1. Case1: 0 degree tilted in both vertical axis and horizontal axis

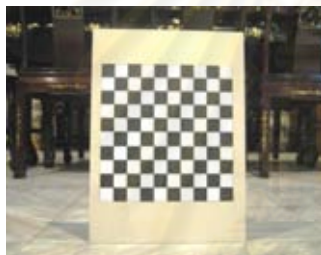
d=30cm



d=45cm



d=60cm



d=75cm

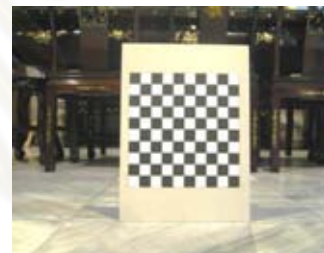


Figure A-1: Images set of Case1

2. Case2: -30 degree tilted in horizontal axis and 0 degree tilted in vertical axis

d=30cm



d=45cm



d=60cm



d=75cm



Figure A-2: Images set of Case2

3. Case3: -45 degree tilted in horizontal axis and 0 degree tilted in vertical axis

d=30cm



d=45cm



d=60cm



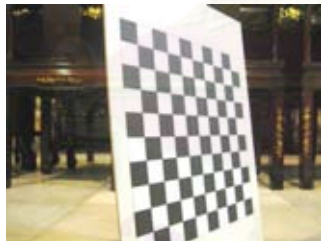
d=75cm



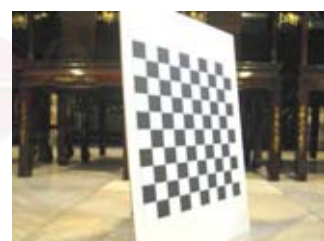
Figure A-3: Images set of Case3

4. Case4: 45 degree tilted in horizontal axis and 0 degree tilted in vertical axis

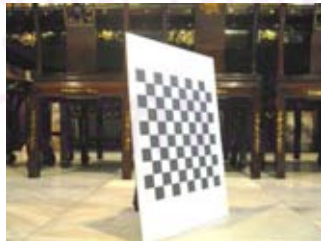
d=30cm



d=45cm



d=60cm



d=75cm



Figure A-4: Images set of Case4

5. Case5: 30 degree tilted in horizontal axis and 60 degree tilted in vertical axis

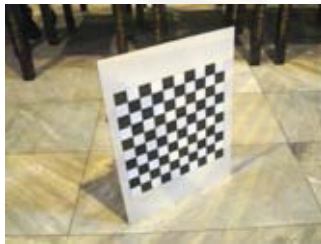
d=30cm



d=45cm



d=60cm



d=75cm



Figure A-5: Images set of Case5

6. Case6: -45 degree tilted in horizontal axis and 60 degree tilted in vertical axis

d=30cm



d=45cm



d=60cm



d=75cm



Figure A-6: Images set of Case6

APPENDIX B

This section shows the details and the pictures of the 3D laser scanner and the equipments. The image of the 3D Laser Scanner design is shown in Figure B-1. The details and specifications of the equipments are shown in Table B-1. The pictures of each component are shown in Figure B-2.

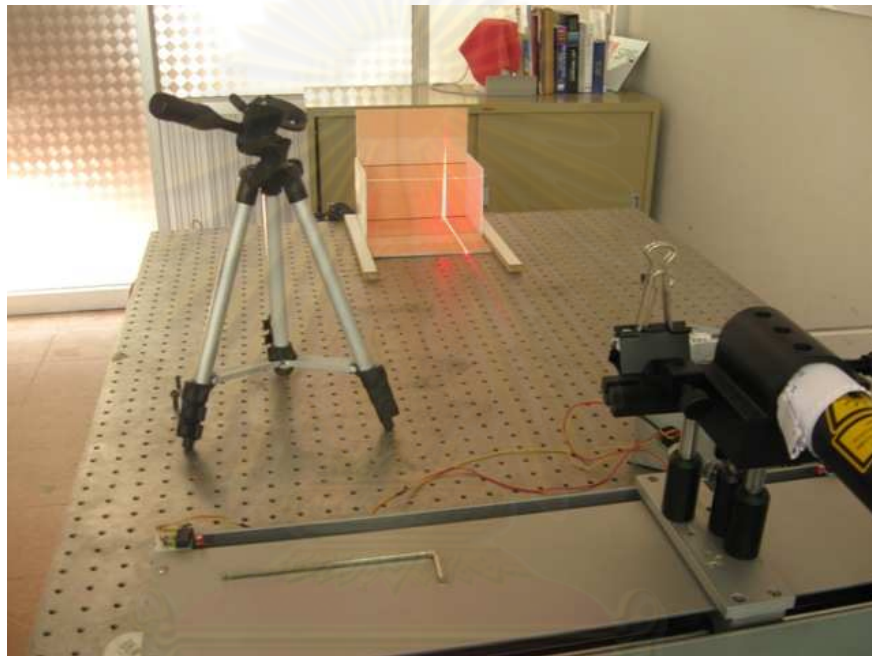


Figure B-1: 3D Laser Scanner

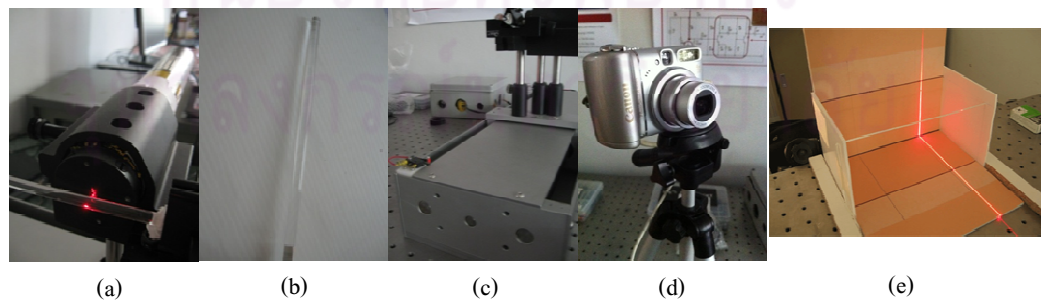
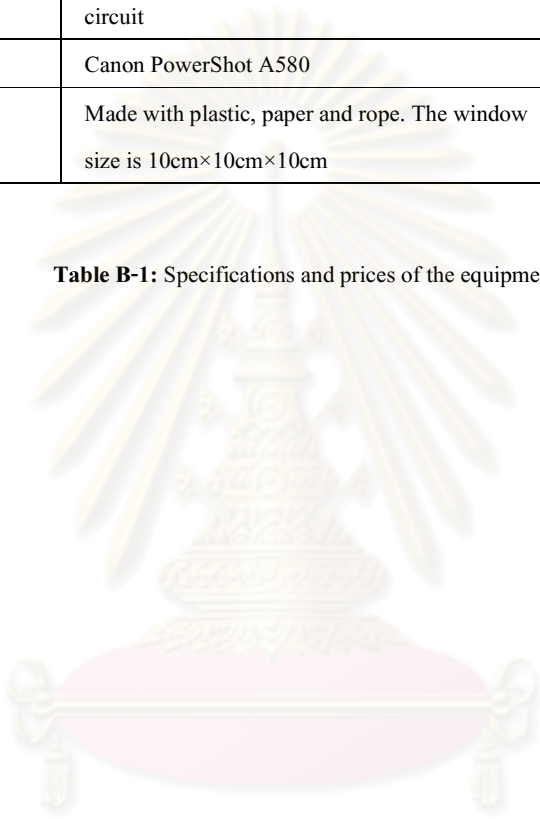


Figure B-2: Images of the setup components (a) laser source (b) cylindrical lens (c) translation stage (d) camera (e) reference box

3D LASER SCANNER COMPONENTS	SPECIFICATION	PRICE (BAHT)
Laser source	He-Ne laser 632.8nm (polarized, 0.8 mW)	30,657.07
Cylindrical lens	Glass rod	10.00
Translation stage	Custom made translation stage with a control circuit	35,000.00
Camera with tri-pod	Canon PowerShot A580	4,990.00
Reference box	Made with plastic, paper and rope. The window size is 10cm×10cm×10cm	30.00
Total		70,687.07

Table B-1: Specifications and prices of the equipments


 ศูนย์วิทยทรัพยากร
 จุฬาลงกรณ์มหาวิทยาลัย

APPENDIX C

This section shows the result images of 3D reconstructed models from the experiments. The number of the tested object is nine. The images of the real object and the reconstructed models are provided. The images on the left side are the real objects. The images on the right side are 3D reconstructed models.

1. Orthogonal planes

Number of vertices: 8,769

Number of faces: 17,167

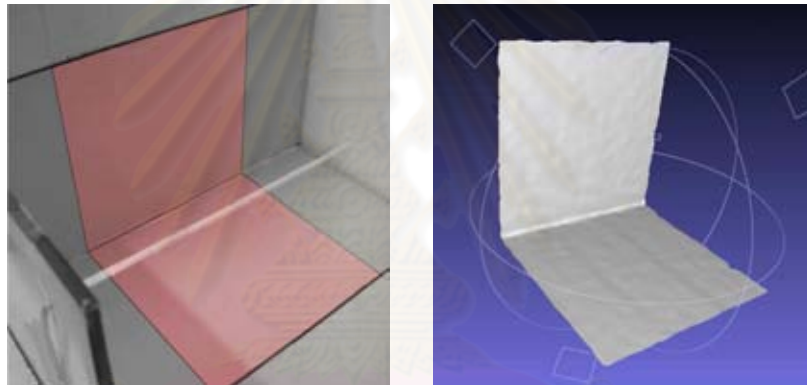


Figure C-1: Real object and reconstructed 3D models of orthogonal planes

2. Cylinder

Number of vertices: 20,533

Number of faces: 38,689



Figure C-2: Real object and reconstructed 3D models of cylinder

3. Rectangular box

Number of vertices: 953

Number of faces: 1,588

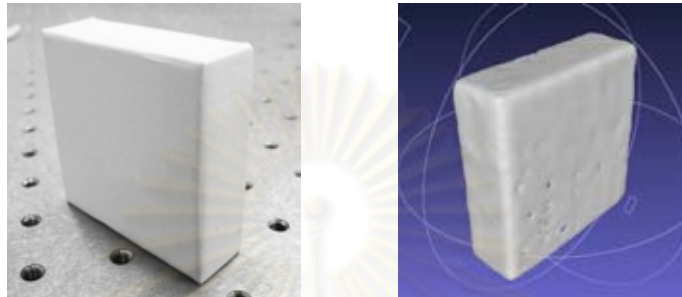


Figure C-3: Real object and reconstructed 3D models of rectangular box

4. Cone

Number of vertices: 9,350

Number of faces: 16,396



Figure C-4: Real object and reconstructed 3D models of cone

5. Sphere

Number of vertices: 5,053

Number of faces: 8,530

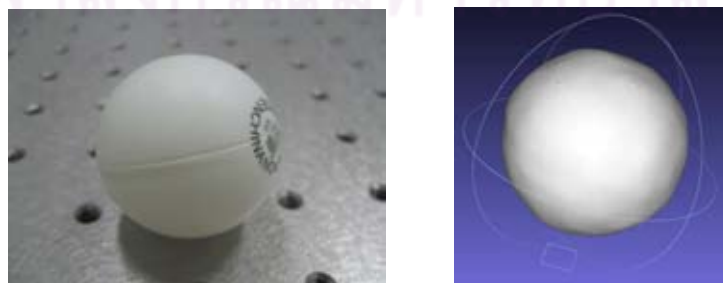


Figure C-5: Real object and reconstructed 3D models of sphere

6. Paper cup

Number of vertices: 267,029

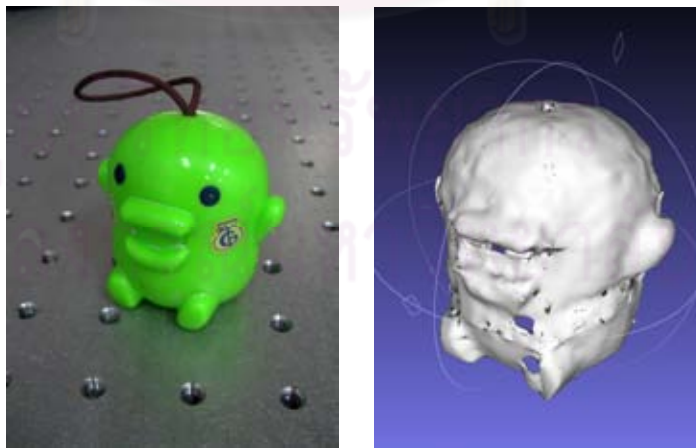
Number of faces: 472,415

**Figure C-6:** Real object and reconstructed 3D models of paper cup

7. Toy

Number of vertices: 76,005

Number of faces: 144,991

**Figure C-7:** Real object and reconstructed 3D models of toy

8. Banana

Number of vertices: 24,973

Number of faces: 45,738

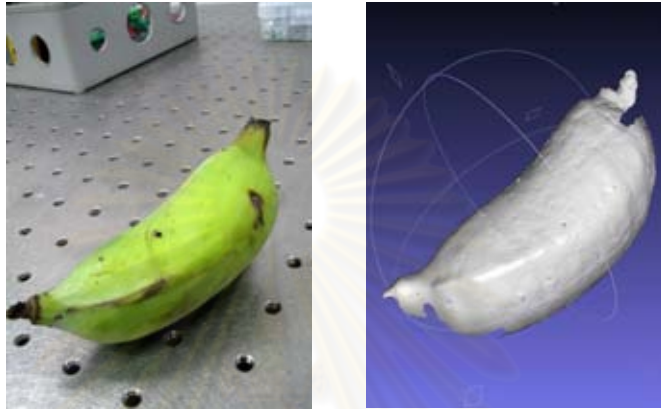


Figure C-8: Real object and reconstructed 3D models of banana

9. Toy

Number of vertices: 20,658

Number of faces: 37,905



Figure C-9: Real object and reconstructed 3D models of toy

Biography

Miss Pimrapat Thanusutiyabhorn graduated in 2004 from Mater Dei Institute, Bangkok, Thailand. She joined Nano-Engineering program at International School of Engineering, Chulalongkorn University in 2005. During the undergraduate studies, she joined SPIE student chapter of Chulalongkorn University and acted as an active member.



ศูนย์วิทยทรัพยากร
จุฬาลงกรณ์มหาวิทยาลัย